

# Robust Design for Multi-Antenna LEO Satellite Communications with Fractional Delay and Doppler Shifts: An RSMA-OTFS Approach

Yunnuo Xu, *Member, IEEE*, Yumeng Zhang, Yijie Mao, *Member, IEEE*,  
Bruno Clerckx, *Fellow, IEEE*, Yun Hee Kim, *Senior Member, IEEE*, Yujun Li, *Member, IEEE*

**Abstract**—Low-Earth-orbit (LEO) satellite communication systems face challenges due to high satellite mobility, which hinders the reliable acquisition of instantaneous channel state information at the transmitter (CSIT) and subsequently degrades multi-user transmission performance. This paper investigates a downlink multi-user multi-antenna system, and tackles the above challenges by introducing orthogonal time frequency space (OTFS) modulation and rate-splitting multiple access (RSMA) transmission. Specifically, OTFS enables stable characterization of time-varying channels by representing them in the delay-Doppler domain. However, realistic propagation introduces various inter-symbol and inter-user interference due to non-orthogonal yet practical rectangular pulse shaping, fractional delays, Doppler shifts, and imperfect (statistical) CSIT. In this context, RSMA offers promising robustness for interference mitigation and CSIT imperfections, and hence is integrated with OTFS to provide a comprehensive solution. A compact cross-domain input-output relationship for RSMA-OTFS is established, and an ergodic sum-rate maximization problem is formulated and solved using a weighted minimum mean-square-error based alternating optimization algorithm that does not depend on channel sparsity. Simulation results reveal that the considered practical propagation effects significantly degrade performance if unaddressed. Furthermore, the RSMA-OTFS scheme demonstrates improved ergodic sum-rate and robustness against CSIT uncertainty across various user deployments and CSIT qualities.

**Index Terms**—Orthogonal time frequency space (OTFS), rate-splitting multiple access (RSMA), multi-user multi-antenna, imperfect CSIT, low-Earth-orbit (LEO) satellite communications

## I. INTRODUCTION

The rapid deployment of Low Earth Orbit (LEO) satellite constellations is reshaping the global communication landscape by enabling broadband access in remote and underserved areas and supporting the development of space-air-ground

integrated networks [1]. Compared with terrestrial communications, LEO satellites operate at low altitudes (typically between 500 km and 2000 km above the Earth), which enables wide-area coverage. However, the high orbital velocity induces high-dynamic time-varying channels, resulting in time and frequency dispersion. These impairments introduce inter-symbol interference, hinder accurate channel estimation, and challenge coherent demodulation [2], [3]. In multi-antenna multi-user systems, such rapidly time-varying channels combined with imperfect channel state information at the transmitter (CSIT) further reduce spatial multiplexing efficiency, complicate precoder design, and impose stringent constraints on interference mitigation [4]. Consequently, system performance degradation caused by these practical impairments cannot be overlooked in LEO communication scenarios [3], [5].

Addressing these challenges requires transmission strategies capable of handling rapid channel variations and mitigating the effects of CSIT uncertainty. Orthogonal time frequency space (OTFS) modulation has emerged as a promising solution for doubly selective channels due to its comprehensive delay-Doppler (DD) domain representation and its ability to exploit full time-frequency (TF) diversity [6]. In parallel, rate-splitting multiple access (RSMA) serves as an effective multiple access technique in managing multi-user interference and enhancing robustness to imperfect CSIT in multi-user multi-antenna networks [7]. The complementary capabilities of the two techniques make their integration an appealing approach for addressing the rapidly time-varying characteristics of LEO system.

Research on OTFS has advanced rapidly in recent years. By converting the time-varying channel in the TF domain into a nearly time-invariant structure in the DD domain, OTFS has demonstrated clear benefits over orthogonal frequency division multiplexing (OFDM) in high-mobility scenarios [6], [8]. The fundamental input-output relationship under single-input single-output (SISO) system and a message-passing detection framework were developed in [8], and subsequent refinements exploited DD domain sparsity to reduce factor-graph iterations while maintaining competitive bit error rate (BER) performance [9]. Further work includes cross-domain detectors that leverage time domain sparsity and DD domain symbol constellation constraints [10], as well as optimized power allocation strategies given frequency-domain zero-forcing (ZF) and minimum mean square error (MMSE) equalizers [11].

Beyond symbol detection, multiple-input multiple-output

Y. Xu and Y. Li are with the School of Information Science and Engineering, Shandong University, Qingdao 266237, China (email: {yunnuo.xu, liyujun}@sdu.edu.cn).

Y. Zhang is with the Department of Electronics and Computer Engineering, The Hong Kong University of Science and Technology, Hong Kong 999077, China (e-mail: eeyzhang@ust.hk).

Y. Mao is with the School of Information Science and Technology, ShanghaiTech University, Shanghai 201210, China (email: maoyj@shanghaitech.edu.cn).

B. Clerckx is with the Department of Electrical and Electronic Engineering at Imperial College London, London SW7 2AZ, UK (email: b.clerckx@imperial.ac.uk).

Y.H. Kim is with the Department of Electronic Engineering and jointly affiliated with the Electronics and Information Convergence Engineering, Kyung Hee University, Yongin 17104, Korea (e-mail: yheekim@khu.ac.kr).

(MIMO)-OTFS has also attracted significant attention for further performance enhancement. Tomlinson-Harashima precoding was introduced in [12] under sparse-channel assumptions, [13] proposed a DD domain precoder based on Hermitian channel structure. More recent contributions such as [14] optimized the signal design to exploit OTFS's potential in dual-functional radar-communication, and [15] developed low-complexity precoding schemes built on simplified channel models. Despite these advancements, most existing studies rely on idealized settings in which the OTFS frame is assumed to be sufficiently large to provide high DD resolution, thereby approximating the continuous delay and Doppler shifts by their integer-valued counterparts. In practical systems, however, fractional Doppler shifts and fractional delays are non-negligible, and together with the use of practical rectangular pulse shaping, they jointly break the canonical doubly block-circulant or sparse structures commonly assumed for OTFS channel matrices [5]. This structural distortion fundamentally limits the applicability of many existing precoding and detection approaches.

Besides the modulation scheme, RSMA is a reliable multiple access strategy to incorporate with OTFS in LEO scenarios, due to its resilience against imperfect CSIT and multi-user interference. Its robustness originates from both its signal structure and its theoretical degree-of-freedom (DoF) optimality under imperfect CSIT. At the transmitter, RSMA linearly precodes rate-split messages, where each user message is divided into a common part decoded by all users and a private part decoded only by its intended user [7], [16], [17]. This structure enables each receiver to successively remove part of the multi-user interference and to reliably decode the remaining private information even when CSIT is inaccurate. From an information-theoretic perspective, RSMA has been proven to achieve the optimal DoF region in a wide range of user configurations with partial CSIT, whereas conventional spatial division multiple access (SDMA) and non-orthogonal multiple access (NOMA) are suboptimal in the same settings. These properties lead to substantial gains in system throughput and reliability, together with improved energy efficiency and reduced transmission latency [18]–[21]. Its robustness to imperfect CSIT makes it particularly suitable for rapidly time-varying environments, with notable benefits demonstrated in satellite communications [22], [23]. When combined with OTFS, RSMA further strengthens the interference management capability and mitigates CSIT-related performance degradation, both of which are critical in practical LEO systems.

Unlike OFDM-based RSMA, applying RSMA to OTFS inherently requires operating in the DD domain, where each symbol spreads across the entire two-dimensional TF plane. This spreading fundamentally changes how precoders interact with data symbols and complicates the design of transmit strategies. Consequently, new precoding and interference management approach is required to accommodate the two-dimensional channel structure of OTFS, rather than relying on the per-subcarrier resource allocation used in OFDM [24]. Several studies have examined the integration of RSMA and OTFS. The work in [25] investigated a cross-domain uplink

design that exploits both TF and DD representations and demonstrated gains in outage performance and user fairness. A downlink extension was presented in [26]. Both works, however, rely on ideal channel models that assume block-circulant structure under bi-orthogonal pulse shaping. Practical rectangular pulse shaping was considered in [27], where fractional Doppler effects were included but fractional delays were omitted. Furthermore, all these studies assume perfect CSIT, which is difficult to obtain in LEO satellite systems due to high mobility and large feedback latency. Most existing work also restricts attention to SISO configurations without precoder optimization, limiting their ability to fully exploit the benefits of multi-antenna configurations and RSMA. As a result, multi-antenna RSMA-OTFS transmission under realistic channel impairments remains insufficiently explored.

Motivated by 1) OTFS and RSMA offer complementary benefits in LEO systems, where OTFS provides resilience to fast channel dynamics, and RSMA improves robustness to interference and CSIT uncertainty, 2) existing studies lack a multi-antenna precoding strategy that comprehensively accounts for the imperfect propagation effect in OTFS LEO networks, this paper develops a RSMA-OTFS transmission framework that considers realistic propagation with fractional delay and Doppler effects, practical non-orthogonal pulse shaping, and imperfect CSIT. The paper, thereby, aims to reduce the gap between theoretical and practical applications in LEO systems. The main contributions of this article are summarized as follows:

- 1) We develop a robust multi-user multi-antenna RSMA-OTFS transmission framework suitable for LEO satellite communications. This framework incorporates practical propagation modelling, including fractional Doppler shifts and delays, practical pulse shaping, and statistical CSIT. It hence extends prior studies that rely on idealized assumptions or SISO settings and establishes a comprehensive study for robust precoder design under CSIT uncertainty.
- 2) Building on the proposed transmission framework, we derive an equivalent cross-domain input-output relationship for multi-antenna RSMA-OTFS systems with statistical CSIT. On this basis, we formulate a sum-rate maximization problem that jointly optimizes the multi-antenna precoders, message splitting, power allocation, and the arrangement matrices that map the precoders into the DD domain. The proposed formulation captures the interaction between common and private message transmission, and enables robust precoder design in the two-dimensional DD domain. To the best of our knowledge, this is the first work to investigate joint precoding and arrangement optimization for multi-antenna RSMA-OTFS transmission under statistical CSIT in LEO satellite systems.
- 3) Due to the non-convex nature of the formulated problem, we transform it into a tractable form through sample average approximation (SAA) and vectorization, and employ a weighted MMSE (WMMSE)-based alternating optimization (AO) algorithm for its solution. The

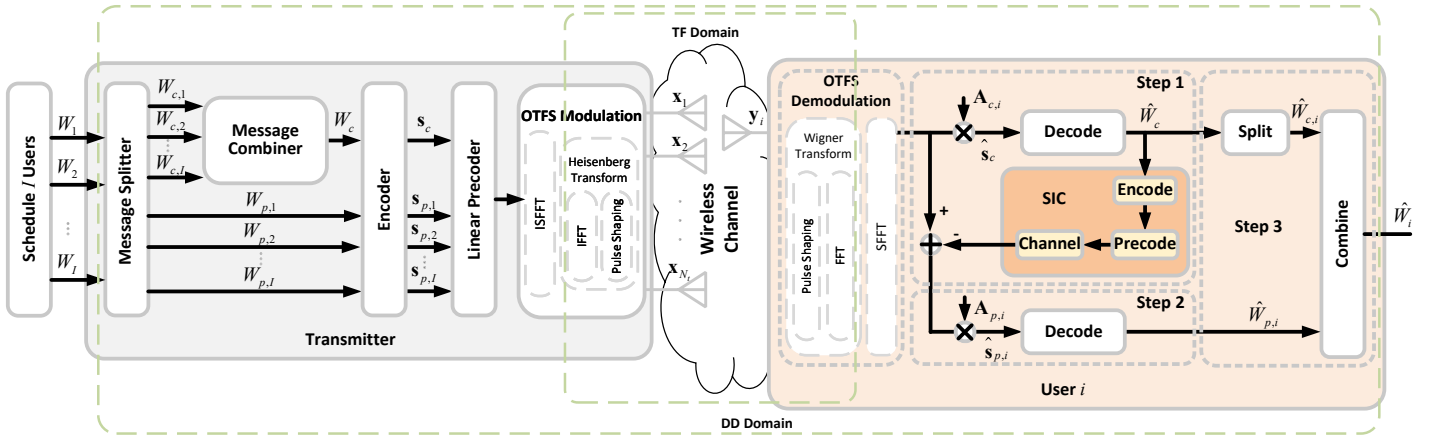


Fig. 1. Transmission model of RSMA-OTFS in multi-user multi-antenna downlink communications.

proposed optimization framework does not rely on a sparse representation of the channel in the DD domain, which enhances its applicability to practical channel assumptions where such sparsity may not hold. Numerical results demonstrate that the multi-antenna RSMA-OTFS design achieves higher ergodic sum-rate (ESR) than existing schemes and provides strong robustness to channel uncertainty and statistical CSIT inaccuracy.

*Organization:* The remainder of this paper is organized as follows. Section II introduces the proposed RSMA-OTFS transmission framework and establishes the corresponding cross-domain input-output relationship. Section III formulates the ESR maximization problem, and Section IV presents the WMMSE-based AO algorithm developed to address the problem. Section V provides the numerical results and performance evaluation. Finally, Section VI concludes the paper.

*Notations:* Matrices, column vectors, and scalars are denoted by boldface uppercase, boldface lowercase, and standard letters, respectively (e.g.,  $\mathbf{A}$ ,  $\mathbf{a}$ ,  $a$ ).  $[\mathbf{A}]_{ij}$  is the  $(i, j)$ -th element of matrix  $\mathbf{A}$ .  $\mathbf{I}_a$  stands for the identity matrix of size  $a \times a$ . The operators  $(\cdot)^T$  and  $(\cdot)^H$  represent transpose and conjugate transpose, respectively. The sets of real and complex numbers are denoted by  $\mathbb{R}$  and  $\mathbb{C}$ , respectively. The absolute value of a scalar is written as  $|\cdot|$ , and  $\|\cdot\|$  denotes the Euclidean norm. The operator  $\text{tr}(\cdot)$  denotes the trace,  $\text{vec}(\cdot)$  is the vectorization operator, and  $\text{vec}^{-1}(\cdot)$  reshapes a vector into a matrix of appropriate dimension. The Kronecker product is written as  $\otimes$ . Expectation is represented by  $\mathbb{E}\{\cdot\}$ , and  $\text{Re}(\cdot)$  denotes the real part of a complex quantity. The notation  $\mathcal{CN}(\zeta, \sigma^2)$  represents a circularly symmetric complex Gaussian random vector with mean  $\zeta$  and covariance matrix  $\sigma^2$ .

## II. SYSTEM MODEL

In this section, we present the system model of a high-speed LEO satellite equipped with an  $N_t$ -antenna uniform linear array (ULA) serving  $I$  single-antenna users simultaneously. The RSMA-OTFS transmission scheme is described below in detail. Fig. 1 illustrates the general architecture of the multi-user, multi-antenna RSMA-OTFS system.

### A. Transmitted Signal

The information symbols are arranged over DD domain with  $N$  Doppler bins and  $M$  delay bins. We denote  $\Delta f$  and  $T = 1/\Delta f$  as the subcarrier spacing and the time slot duration, respectively. The OTFS signal frame is set to  $T_f = NT$  s duration and  $B = M\Delta f$  Hz bandwidth.

According to RSMA<sup>1</sup>, each user's message is split into common and private parts,  $W_{c,i}, W_{p,i}, \forall i \in \mathcal{I} = \{1, 2, \dots, I\}$ . The common parts of all users' messages are combined into a single common message and encoded into a common stream, arranged in DD domain  $\mathbf{S}_c \in \mathbb{C}^{M \times N}$ . The private message of user- $i$  is encoded into private stream arranged in DD domain  $\mathbf{S}_{p,i} \in \mathbb{C}^{M \times N}$ . Correspondingly, we define  $\mathbf{s}_c = \text{vec}(\mathbf{S}_c) \in \mathbb{C}^{MN \times 1}$ , and  $\mathbf{s}_{p,i} = \text{vec}(\mathbf{S}_{p,i}) \in \mathbb{C}^{MN \times 1}, \forall i \in \mathcal{I}$ . We assume that the symbol power is normalized. The common and private symbols for all users are first precoded in the DD domain symbols as follows

$$\mathbf{X}^{\text{DD}} = \Psi_c \mathbf{s}_c \mathbf{p}_c^T + \sum_{i=1}^I \Psi_{p,i} \mathbf{s}_{p,i} \mathbf{p}_{p,i}^T, \quad (1)$$

where  $\Psi_c \in \mathbb{R}^{MN \times MN}$  and  $\Psi_{p,i} \in \mathbb{R}^{MN \times MN}$  are diagonal binary arrangement matrices that map the symbols into the corresponding positions in  $\mathbf{X}^{\text{DD}}$ , and  $\mathbf{p}_c$  and  $\mathbf{p}_{p,i} \in \mathbb{C}^{N_t \times 1}$  are the precoding vectors for common and private symbols, respectively. Denote  $\mathbf{P}_{BF} = [\mathbf{p}_c, \mathbf{p}_{p,1}, \dots, \mathbf{p}_{p,I}]^T$  and  $\Psi = \{\Psi_c, \Psi_{p,1}, \dots, \Psi_{p,I}\}$ . Then, the vectorized DD domain transmitted symbols for all antennas is expressed as

$$\begin{aligned} \mathbf{x}^{\text{DD}} &= \text{vec}(\mathbf{X}^{\text{DD}}) \\ &= (\mathbf{p}_c \otimes \Psi_c) \mathbf{s}_c + \sum_{i=1}^I (\mathbf{p}_{p,i} \otimes \Psi_{p,i}) \mathbf{s}_{p,i}. \end{aligned} \quad (2)$$

The transmit power is constrained by  $P_t$ , i.e.,  $\mathbb{E}\{\mathbf{P}_{BF} \mathbf{P}_{BF}^H\} \leq P_t$ . Then DD domain symbols  $\mathbf{X}^{\text{DD}}$  are sequentially transformed into TF and time-delay (TD) symbols, denoted as  $\mathbf{X}^{\text{TF}}$  and  $\mathbf{X}^{\text{TD}}$ , through inverse symplectic finite Fourier transform

<sup>1</sup>In this study, we adopt 1-layer RSMA framework, where all common parts are combined into one common message [28], [29].

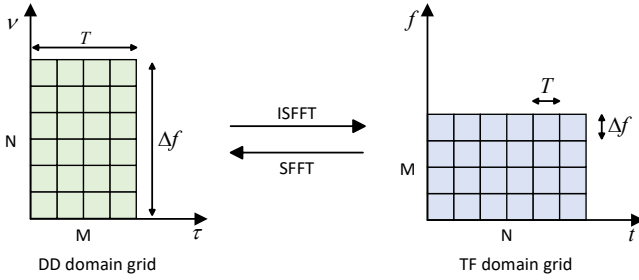


Fig. 2. DD domain and TF domain transformation.

(ISFFT) and the Heisenberg transform, respectively [6], [12]. This process can be expressed as

$$\mathbf{X}^{\text{TF}} = (\mathbf{F}_N^H \otimes \mathbf{F}_M) \mathbf{X}^{\text{DD}}, \quad (3a)$$

$$\mathbf{X}^{\text{TD}} = \mathbf{G}_{tx} [(\mathbf{I}_N \otimes \mathbf{F}_M^H) \mathbf{X}^{\text{TF}}] = (\mathbf{F}_N^H \otimes \mathbf{I}_M) \mathbf{X}^{\text{DD}}, \quad (3b)$$

where  $\mathbf{G}_{tx} = \mathbf{I}_{MN}$  for the rectangular shape [30] while  $\mathbf{F}_M \in \mathbb{C}^{M \times M}$  and  $\mathbf{F}_N \in \mathbb{C}^{N \times N}$  are normalized discrete Fourier transform (DFT) matrices. The transformation between the DD domain and the TF domain is shown in Fig. 2. The vectorized transmitted symbols in the TD domain can be defined as

$$\begin{aligned} \mathbf{x}^{\text{TD}} &= \text{vec}(\mathbf{X}^{\text{TD}}) \\ &= [\mathbf{p}_c \otimes (\mathbf{F}_N^H \otimes \mathbf{I}_M) \tilde{\Psi}_c] \mathbf{s}_c + \sum_{i=1}^I [\mathbf{p}_{p,i} \otimes (\mathbf{F}_N^H \otimes \mathbf{I}_M) \tilde{\Psi}_{p,i}] \mathbf{s}_{p,i} \\ &= (\mathbf{p}_c \otimes \tilde{\Psi}_c) \mathbf{s}_c + \sum_{i=1}^I (\mathbf{p}_{p,i} \otimes \tilde{\Psi}_{p,i}) \mathbf{s}_{p,i}, \end{aligned} \quad (4)$$

where  $\tilde{\Psi}_c$  and  $\tilde{\Psi}_{p,i}$  are denoted as effective arrangement matrices in TD domain.

## B. Received Signal

At  $i$ -th user, the received TD domain signal is expressed as

$$\mathbf{y}_i^{\text{TD}} = \mathbf{H}_i^{\text{TD}} \mathbf{x}^{\text{TD}} + \mathbf{n}_i \in \mathbb{C}^{MN \times 1} \quad (5)$$

where  $\mathbf{H}_i^{\text{TD}} \in \mathbb{C}^{MN \times MN}$  is the TD domain channel matrix between the satellite and user- $i$ , and  $\mathbf{n}_i \in \mathbb{C}^{MN \times 1}$  is the additive white gaussian noise (AWGN) vector of user  $i$  with  $\mathbf{n}_i \sim \mathcal{CN}(0, \sigma_{n,i}^2 \mathbf{I}_{MN})$ . Then, the received signal is reshaped into the following matrix representation  $\mathbf{Y}_i^{\text{TD}} = \text{vec}^{-1}(\mathbf{y}_i^{\text{TD}})$ , where  $\mathbf{Y}_i^{\text{TD}} \in \mathbb{C}^{M \times N}$  denotes the received OTFS frame in the TD domain.

To obtain its representation in the TF domain, Wigner transform (filtering pulse followed by a fast Fourier transform (FFT)) is applied, yielding

$$\mathbf{Y}_i^{\text{TF}} = \mathbf{F}_M \mathbf{G}_{rx} \mathbf{Y}_i^{\text{TD}}, \quad (6)$$

where  $\mathbf{G}_{rx}$  denotes the pulse-shaping matrix associated with the receiver filter. Similar to  $\mathbf{G}_{tx}$ , the receiver pulse is taken to be an identity matrix.

Subsequently, the symplectic finite Fourier transform (SFFT) is employed to map the TF domain signal into the DD domain:

$$\mathbf{Y}_i^{\text{DD}} = \mathbf{F}_M^H \mathbf{Y}_i^{\text{TF}} \mathbf{F}_N = \mathbf{Y}_i^{\text{TD}} \mathbf{F}_N. \quad (7)$$

In the vectorized form, the input–output relationship in the DD domain can be expressed as

$$\mathbf{y}_i^{\text{DD}} = (\mathbf{F}_N \otimes \mathbf{I}_M) \mathbf{H}_i^{\text{TD}} \mathbf{x}^{\text{TD}} + \mathbf{n}_i, \quad (8a)$$

$$\begin{aligned} &= (\mathbf{F}_N \otimes \mathbf{I}_M) \mathbf{H}_i^{\text{TD}} (\mathbf{p}_c \otimes \tilde{\Psi}_c) \mathbf{s}_c \\ &+ \sum_{i=1}^I (\mathbf{F}_N \otimes \mathbf{I}_M) \mathbf{H}_i^{\text{TD}} (\mathbf{p}_{p,i} \otimes \tilde{\Psi}_{p,i}) \mathbf{s}_{p,i} + \mathbf{n}_i \end{aligned} \quad (8b)$$

$$= \tilde{\mathbf{H}}_i^{\text{DD}} \tilde{\mathbf{P}}_c \mathbf{s}_c + \sum_{i=1}^I \tilde{\mathbf{H}}_i^{\text{DD}} \tilde{\mathbf{P}}_{p,i} \mathbf{s}_{p,i} + \mathbf{n}_i, \quad (8c)$$

with

$$\tilde{\mathbf{H}}_i^{\text{DD}} = (\mathbf{F}_N \otimes \mathbf{I}_M) \mathbf{H}_i^{\text{TD}}, \quad (9a)$$

$$\tilde{\mathbf{P}}_j = \mathbf{p}_j \otimes \tilde{\Psi}_j, j \in \{c, \{p, i\}_{i=1}^I\}. \quad (9b)$$

$\tilde{\mathbf{H}}_i^{\text{DD}}$  represents the effective DD domain channel, and  $\tilde{\mathbf{P}}_j$  denotes the effective TD domain precoding matrix. Note that (9b) transfers the DD domain precoder,  $\mathbf{p}_j^T$ , to effective TD domain precoder,  $\tilde{\mathbf{P}}_j$ ,  $j \in \{c, \{p, i\}_{i=1}^I\}$ .

*Remark 1:* In this paper, we claim (8c) as a cross-domain modeling as it features a mixed TD ( $\tilde{\mathbf{P}}_j$ ) and DD ( $\tilde{\mathbf{H}}_i^{\text{DD}}$ ) expression, yet enabling a decoupling relationship between them, which constitutes one of the novelties of the proposed framework. The decoupled precoding and channel matrices provides a more tractable optimization problem as it will be detailed in Section IV. In contrast, conventional approaches typically adopt a full DD domain representation [12], [13], which is expressed as

$$\mathbf{y}_i^{\text{DD}} \triangleq \mathbf{H}_{c,i}^{\text{DD,con}} \mathbf{s}_c + \sum_{i=1}^I \mathbf{H}_{p,i}^{\text{DD,con}} \mathbf{s}_{p,i} + \mathbf{n}_i, \quad (10)$$

where  $\mathbf{H}_{k,i}^{\text{DD,con}} = (\mathbf{F}_N \otimes \mathbf{I}_M) \mathbf{H}_{k,i}^{\text{TD}} (\mathbf{p}_k \otimes \tilde{\Psi}_k)$ ,  $k \in \{c, p\}$ . Such a formulation couples the precoder with the channel response, which complicates the subsequent precoder design.

*Remark 2:* Compared to RSMA-OFDM in [24], RSMA-OTFS introduces extra Doppler domain, making each symbol in  $\mathbf{s}_c$  and  $\mathbf{s}_{p,i}$  spread over the entire two-dimensional TF plane. This results in the multi-antenna precoding vector  $\mathbf{p}_j$  being expanded to the Kronecker-structured precoder  $\tilde{\mathbf{P}}_j$ , which requires joint waveform shaping across antennas and across the whole two-dimensional OTFS frame. In effect, each data stream is embedded in the entire frame rather than confined to a particular subcarrier or time slot, which improves robustness under rapidly time-varying LEO satellite channels.

## C. Channel Model

The DD domain channel between the satellite and user- $i$  is modeled as a sum of line of sight (LoS) and non-line of sight (NLoS) paths [31], [32], which is expressed as

$$\begin{aligned} \mathbf{h}_i^{\text{DD}}(\tau, \nu) &= \sqrt{\frac{\gamma_i}{\gamma_i + 1}} h_i^{\text{LoS}} \mathbf{a}^T(\theta_i^{\text{LoS}}) \delta(\tau - \tau_i^{\text{LoS}}) \delta(\nu - \nu_i^{\text{LoS}}) \\ &+ \sqrt{\frac{1}{\gamma_i + 1}} \sum_{q=1}^{Q_i} h_{i,q}^{\text{NLoS}} \mathbf{a}^T(\theta_{i,q}^{\text{NLoS}}) \delta(\tau - \tau_{i,q}^{\text{NLoS}}) \delta(\nu - \nu_{i,q}^{\text{NLoS}}), \end{aligned} \quad (11)$$

where the LoS component is characterized by complex path gain  $h_i^{\text{LoS}}$ , angle of departure (AoD)  $\theta_i^{\text{LoS}}$ , propagation delay  $\tau_i^{\text{LoS}}$ , and Doppler shift  $\nu_i^{\text{LoS}}$ ; the  $q$ -th NLoS path is described by  $h_{i,q}^{\text{NLoS}}$ ,  $\theta_{i,q}^{\text{NLoS}}$ ,  $\tau_{i,q}^{\text{NLoS}}$ , and  $\nu_{i,q}^{\text{NLoS}}$ , representing the multipath gain, AoD, propagation delay, and Doppler shift, respectively;  $\gamma_i$  denotes the Rician factor that governs the power ratio between the LoS and scattered components;  $Q_i$  is the total number of NLoS paths; and  $\mathbf{a} \in \mathbb{C}^{N_t \times 1}$  denotes the spatial array steering vector of the ULA for the LEO satellite. The parameters are elaborated upon in the subsequent discussion.

1) *Path gain*: The terrestrial-satellite link is characterized by sparse scattering, leading to a dominant LoS component and weak NLoS paths, which are captured by Rician factor  $\gamma_i$ . Denote the LoS gain as  $h_i^{\text{LoS}} = e^{j\varphi_i}$  with  $\varphi_i \sim \mathcal{U}(0, 2\pi)$ , and NLoS gains follow  $h_{i,q}^{\text{NLoS}} \sim \mathcal{CN}(0, \sigma_{i,q}^2)$ .

2) *Spatial array steering vector*: The ULA steering vector is given by

$$\mathbf{a}(\theta_{i,q}) = \left[ e^{-j2\pi \frac{d}{\lambda} \sin(\theta_{i,q}) \mathbf{n}_t} \right]^T, \quad (12)$$

where  $\mathbf{n}_t = [0, 1, \dots, N_t - 1]$ ,  $\lambda$  is the carrier wavelength, and  $d = \lambda/2$  is the antenna spacing.

3) *Doppler shift and Delay*: The Doppler shift  $\nu_i^{\text{LoS}}$ , associated with the LoS component of user- $i$  is dominated by two independent Doppler shifts,  $\nu_i^{\text{LoS-S}}$  and  $\nu_i^{\text{LoS-U}}$ , which result from the movements of the LEO satellite and user, respectively. Given the high velocity of the LEO satellite, the Doppler shift,  $\nu_i^{\text{LoS}}$ , is primarily determined by the satellite's motion, leading to  $\nu_i^{\text{LoS}} \approx \nu_i^{\text{LoS-S}}$ . Similarly, we have the Doppler shifts of NLoS paths,  $\nu_{i,q}^{\text{NLoS}}$ , are largely governed by the satellite's velocity, resulting in  $\nu_{i,q}^{\text{NLoS}} \approx \nu_{i,q}^{\text{NLoS-S}}$ . We assume that most of the propagation delay is compensated through configuring the timing advance information at each user, and the remaining delay offset is limited to the symbol level [33], [34].

For notational simplicity, the LoS path is indexed as  $q = 0$ , with effective gain  $h_{i,0} = \sqrt{\frac{\gamma_i}{\gamma_i+1}} h_i^{\text{LoS}}$ ,  $\theta_{i,0} = \theta_i^{\text{LoS}}$ , delay  $\tau_{i,0} = \tau_i^{\text{LoS}}$  and Doppler shift  $\nu_{i,0} = \nu_i^{\text{LoS}}$ . For  $q = 1, \dots, Q_i$ , NLoS components are defined as  $h_{i,q} = \sqrt{\frac{1}{\gamma_i+1}} h_{i,q}^{\text{NLoS}}$ ,  $\theta_{i,q} = \theta_{i,q}^{\text{NLoS}}$ ,  $\tau_{i,q} = \tau_{i,q}^{\text{NLoS}}$  and  $\nu_{i,q} = \nu_{i,q}^{\text{NLoS}}$ . The DD domain channel is expressed as

$$\mathbf{h}_i^{\text{DD}}(\tau, \nu) = \sum_{q=0}^{Q_i} h_{i,q} \mathbf{a}(\theta_{i,q}) \delta(\tau - \tau_{i,q}) \delta(\nu - \nu_{i,q}). \quad (13)$$

To better capture practical channel characteristics, both fractional delay, and fractional Doppler shifts are considered. Accordingly, the delay and Doppler shift of the  $q$ -th path for the  $i$ -th user are expressed as

$$\tau_{i,q} = \frac{l_{i,q} + \ell_{i,q}}{M\Delta f}, \quad \nu_{i,q} = \frac{k_{i,q} + \kappa_{i,q}}{NT}, \quad (14)$$

where  $l_{i,q}$  and  $k_{i,q}$  denote the integer delay and Doppler indices, while  $\ell_{i,q}, \kappa_{i,q} \in (-\frac{1}{2}, \frac{1}{2})$  represent the corresponding fractional components. We assume the maximal delay and maximal Doppler of the propagation path is bounded, i.e.,  $\tau_{\max} \leq T$  and  $\nu_{\max} \leq \Delta f$ .

The TD domain channel corresponding to (13) can be expressed in an equivalent matrix form as

$$\mathbf{H}_i^{\text{TD}} = \sum_{q=0}^{Q_i} h_{i,q} e^{-j2\pi \frac{(k_{i,q} + \kappa_{i,q})(l_{i,q} + \ell_{i,q})}{MN}} \left[ \mathbf{a}(\theta_{i,q}) \otimes \check{\mathbf{H}}_{i,q}^{\text{TD}} \right], \quad (15)$$

where  $\check{\mathbf{H}}_{i,q}^{\text{TD}} = \mathbf{\Delta}_{i,q} \mathbf{\Xi}_{i,q}$ , and the matrices  $\mathbf{\Delta}_{i,q} \in \mathbb{C}^{MN \times MN}$  and  $\mathbf{\Xi}_{i,q} \in \mathbb{C}^{MN \times MN}$  capture the effects of Doppler shifts and delay, respectively [5]. The Doppler effects matrix  $\mathbf{\Delta}_{i,q}$  is a diagonal matrix with diagonal elements defined as

$$\begin{aligned} & [\mathbf{\Delta}_{i,q}]_{n'+Nm', n'+Nm'} \\ &= \exp \left( j2\pi \frac{k_{i,q} + \kappa_{i,q}}{N} (n' + \frac{m'}{M}) \right). \end{aligned} \quad (16)$$

The  $(n'+Nm', n+Nm)$ -th element of the delay effects matrix  $\mathbf{\Xi}_{i,q}$  is

$$\begin{aligned} & [\mathbf{\Xi}_{i,q}]_{n'+Nm', n+Nm} \\ &= \text{sinc} \left( M(n' - n) + m' - m - l_{q,i} - \ell_{q,i} \right), \end{aligned} \quad (17)$$

The overall channel response across all users is represented as

$$\mathbf{H}^{\text{TD}} = [\mathbf{H}_1^{\text{TD}}, \mathbf{H}_2^{\text{TD}}, \dots, \mathbf{H}_I^{\text{TD}}], \quad (18)$$

where  $\mathbf{H}_i^{\text{TD}}$  denotes the channel matrix associated with the  $i$ -th user.

#### D. Channel State Information

In practical satellite communication systems, perfect channel state information (CSI) acquisition is infeasible due to several factors such as hardware impairments, and estimation errors [35], [36]. Consequently, the satellite (transmitter) has access only to a partial and imperfect channel knowledge. The actual channel is modeled as the sum of the estimated channel and an error component<sup>2</sup> [37], [38]

$$\mathbf{H}_i = \hat{\mathbf{H}}_i + \mathbf{E}_{h,i}, \quad (19)$$

where  $\mathbf{E}_{h,i}$  captures the estimation uncertainty for user  $i$ , modeled as

$$\mathbf{E}_{h,i} = \sum_{q=0}^{Q_i} e_{i,q} e^{-j2\pi \frac{(k_{i,q} + \kappa_{i,q})(l_{i,q} + \ell_{i,q})}{MN}} \left[ \mathbf{a}(\theta_{i,q}) \otimes \check{\mathbf{H}}_i \right] \quad (20)$$

with  $e_{i,q} \sim \mathcal{CN}(0, \sigma_{h,ei}^2)$  denoting the estimation error of the  $q$ -th path gain for user  $i$ . The variance of the path-gain estimation error is given by  $\sigma_{h,ei}^2 = \rho^2 \gamma_e + \frac{1-\rho^2}{Q_i}$ , where  $\rho$  is the correlation coefficient between the estimated and actual channel gains, and  $\gamma_e$  denotes the signal-to-noise ratio (SNR) of the pilot signal.

We further assume that the joint distribution  $(\mathbf{H}, \hat{\mathbf{H}})$  is stationary and ergodic [28], and that the conditional distribution  $f_{\mathbf{H}|\hat{\mathbf{H}}}(\mathbf{H} | \hat{\mathbf{H}})$  is known at the transmitter side, while the instantaneous realization of  $\hat{\mathbf{H}}$  remains unknown during transmission, corresponding to statistical CSIT and perfect channel state information at the receiver (CSIR) conditions. In this work, we mainly focus on the estimation errors that occur in the path gains,  $e_{i,q}$ .

<sup>2</sup>For notational simplicity, the domain superscripts (e.g., DD or TD) of the channel are omitted throughout this subsection.

$$\mathbf{T}_{c,i} \triangleq \mathbb{E} \left\{ \mathbf{y}_i^{\text{DD}} \mathbf{y}_i^{\text{DD}H} \right\} = \underbrace{\tilde{\mathbf{H}}_i^{\text{DD}} \tilde{\mathbf{P}}_c \tilde{\mathbf{P}}_c^H (\tilde{\mathbf{H}}_i^{\text{DD}})^H}_{\mathbf{S}_{c,i}} + \underbrace{\sum_{i'=1}^I \tilde{\mathbf{H}}_i^{\text{DD}} \tilde{\mathbf{P}}_{p,i'} \tilde{\mathbf{P}}_{p,i'}^H (\tilde{\mathbf{H}}_i^{\text{DD}})^H}_{\mathbf{K}_{c,i}} + \mathbf{I}_{MN}, \quad (21a)$$

$$\mathbf{T}_{p,i} \triangleq \mathbb{E} \left\{ (\mathbf{y}_i^{\text{DD}} - \tilde{\mathbf{H}}_i^{\text{DD}} \tilde{\mathbf{P}}_c \mathbf{s}_c) (\mathbf{y}_i^{\text{DD}} - \tilde{\mathbf{H}}_i^{\text{DD}} \tilde{\mathbf{P}}_c \mathbf{s}_c)^H \right\} = \underbrace{\tilde{\mathbf{H}}_i^{\text{DD}} \tilde{\mathbf{P}}_{p,i} \tilde{\mathbf{P}}_{p,i}^H (\tilde{\mathbf{H}}_i^{\text{DD}})^H}_{\mathbf{S}_{p,i}} + \underbrace{\sum_{i'=1, i' \neq i}^I \tilde{\mathbf{H}}_i^{\text{DD}} \tilde{\mathbf{P}}_{p,i'} \tilde{\mathbf{P}}_{p,i'}^H (\tilde{\mathbf{H}}_i^{\text{DD}})^H}_{\mathbf{K}_{p,i}} + \mathbf{I}_{MN}. \quad (21b)$$

### E. Achievable Rate

At user  $i$ , signal detection is carried out following the successive interference cancellation (SIC) strategy. Specifically, the user first decodes the common stream vector  $\mathbf{s}_c$  while treating interference from all private streams as noise. Once the common stream is successfully recovered and removed, user  $i$  proceeds to decode its intended private stream vector  $\mathbf{s}_{p,i}$ , where the remaining interference from other users private streams is regarded as noise. The recovered message for user  $i$  is obtained by combining the decoded portion of the common stream with its private stream. In the following, we derive the instantaneous and achievable ergodic rate for both the common and private streams, referred as the common rate and private rate, respectively.

The covariance matrices of the received signals corresponding to the common and private streams of user  $i$  are defined in (21a) and (21b), respectively, as shown at the top of this page.

Since the transmitter determines its precoders based on the estimated channel state  $\hat{\mathbf{H}}_i^{\text{DD}}$ , while each user decodes its signals using the actual channel realization  $\mathbf{H}_i^{\text{DD}}$  with perfect CSIR, the pair  $(\hat{\mathbf{H}}_i^{\text{DD}}, \mathbf{H}_i^{\text{DD}})$  jointly determines the instantaneous achievable rates of the common and private streams. Assuming Gaussian signaling, the instantaneous signal to interference-plus-noise ratio (SINR) of the common and private streams at user  $i$  are given by

$$\Gamma_{c,i} = \tilde{\mathbf{P}}_c^H (\tilde{\mathbf{H}}_i^{\text{DD}})^H \mathbf{K}_{c,i}^{-1} \tilde{\mathbf{H}}_i^{\text{DD}} \tilde{\mathbf{P}}_c, \quad (22a)$$

$$\Gamma_{p,i} = \tilde{\mathbf{P}}_{p,i}^H (\tilde{\mathbf{H}}_i^{\text{DD}})^H \mathbf{K}_{p,i}^{-1} \tilde{\mathbf{H}}_i^{\text{DD}} \tilde{\mathbf{P}}_{p,i}. \quad (22b)$$

the corresponding instantaneous achievable rates for user  $i$  are expressed as

$$R_{c,i} = \frac{1}{MN} \log_2 \det (\mathbf{I}_{MN} + \Gamma_{c,i}), \quad (23a)$$

$$R_{p,i} = \frac{1}{MN} \log_2 \det (\mathbf{I}_{MN} + \Gamma_{p,i}). \quad (23b)$$

Since the transmitter only has partial CSIT, relying on instantaneous rates may overestimate system performance [28]. To capture the average performance, we define ergodic rate of the common and private streams as

$$\bar{R}_{c,i} = \mathbb{E}_{(\mathbf{H}_i^{\text{DD}}, \hat{\mathbf{H}}_i^{\text{DD}})} \{R_{c,i}\}, \quad \bar{R}_{p,i} = \mathbb{E}_{(\mathbf{H}_i^{\text{DD}}, \hat{\mathbf{H}}_i^{\text{DD}})} \{R_{p,i}\}, \quad (24)$$

where the expectation is taken over the joint distribution of  $(\mathbf{H}_i^{\text{DD}}, \hat{\mathbf{H}}_i^{\text{DD}})$ . To ensure that all users can decode the common stream, the common ergodic rate must satisfy  $\bar{R}_c =$

$\min_{i \in \mathcal{I}} \bar{R}_{c,i}$ . The common rate  $\bar{R}_c$  is shared among users as  $\sum_{i \in \mathcal{I}} \bar{C}_i = \bar{R}_c$ , and the total ergodic rate achieved by user  $i$  is given by  $\bar{R}_{\text{tot},i} = \bar{C}_i + \bar{R}_{p,i}$ .

### III. PROBLEM FORMULATION

In this section, we formulate an ESR maximization problem for the considered system.

To illustrate the impact of channel uncertainty, we first consider a baseline strategy where the transmitter relies on the estimated channel  $\hat{\mathbf{H}}_i^{\text{DD}}$  and determines the instantaneous precoder  $\mathbf{P}_{\text{BF}}$  by maximizing the instantaneous sum-rate under the power constraint  $\text{tr}(\mathbf{P}_{\text{BF}} \mathbf{P}_{\text{BF}}^H) \leq P_t$ . While this approach is intuitive, it implicitly assumes that the channel estimate is accurate. In practice, however, estimation errors create a mismatch between the adopted precoder and the actual channel realization. Such mismatch is particularly detrimental in multi-user settings, where inaccurate channel knowledge may cause the transmitter to select rates that cannot be reliably decoded, resulting in performance degradation [28]. These considerations motivate an optimization framework that explicitly accounts for CSIT uncertainty when determining the transmission strategy.

To capture the long-term behavior of the system under such uncertainty, we focus on maximizing the ESR, which reflects the achievable performance averaged over all channel realizations and provides a more robust performance measure than instantaneous rate optimization. For the RSMA-OTFS transmission strategy, the ESR is denoted as  $\bar{R} = \sum_{i=1}^I \bar{R}_{\text{tot},i}$ . Since the instantaneous rate cannot be perfectly obtained under imperfect CSIT, the transmitter relies on the average rate, which represents the short-term expectation conditioned on the estimated channel.

For a given channel estimate  $\hat{\mathbf{H}}_i^{\text{DD}}$  and its corresponding precoder  $\mathbf{P}_{\text{BF}}(\hat{\mathbf{H}}_i^{\text{DD}})$ , the conditional average rate is defined as the conditional expectation of the instantaneous rate with respect to the CSIT error distribution:

$$\hat{R}_{c,i}(\hat{\mathbf{H}}_i^{\text{DD}}) = \mathbb{E}_{\mathbf{H}_i^{\text{DD}} | \hat{\mathbf{H}}_i^{\text{DD}}} \left\{ R_{c,i}(\mathbf{H}_i^{\text{DD}}, \hat{\mathbf{H}}_i^{\text{DD}}) \mid \hat{\mathbf{H}}_i^{\text{DD}} \right\}, \quad (25a)$$

$$\hat{R}_{p,i}(\hat{\mathbf{H}}_i^{\text{DD}}) = \mathbb{E}_{\mathbf{H}_i^{\text{DD}} | \hat{\mathbf{H}}_i^{\text{DD}}} \left\{ R_{p,i}(\mathbf{H}_i^{\text{DD}}, \hat{\mathbf{H}}_i^{\text{DD}}) \mid \hat{\mathbf{H}}_i^{\text{DD}} \right\}. \quad (25b)$$

The conditional average rate differs from the ergodic rate because the former represents the expected rate under a specific channel estimate, while the latter characterizes the

long-term average over all joint channel realizations. According to the law of total expectation, their relationship can be expressed as  $\bar{R}_{c,i} = \mathbb{E}_{\hat{\mathbf{H}}_i^{\text{DD}}} \left\{ \hat{R}_{c,i}(\hat{\mathbf{H}}_i^{\text{DD}}) \right\}$ ,  $\bar{R}_{p,i} = \mathbb{E}_{\hat{\mathbf{H}}_i^{\text{DD}}} \left\{ \hat{R}_{p,i}(\hat{\mathbf{H}}_i^{\text{DD}}) \right\}$ . For the common stream, let  $\hat{C}_i$  denote the average rate portion of user- $i$ , satisfying  $\sum_{i=1}^I \hat{C}_i = \hat{R}_c$ , where  $\hat{R}_c \leq \min_{i \in \mathcal{I}} \{ \hat{R}_{c,i} \}$ . Moreover, the inequality  $\min_{i \in \mathcal{I}} \left\{ \mathbb{E}_{\hat{\mathbf{H}}_i^{\text{DD}}} [\hat{R}_{c,i}] \right\} \geq \mathbb{E}_{\hat{\mathbf{H}}_i^{\text{DD}}} \left[ \min_{i \in \mathcal{I}} \{ \hat{R}_{c,i} \} \right]$ , follows from the fact that exchanging the expectation and minimization operations cannot increase the result [28].

By invoking the law of large numbers (LLN), the ergodic rate can be approximated by averaging the average rate over all estimated channel states, thus decoupling dependencies across channel realizations. Consequently, the long-term ESR maximization problem under imperfect CSIT can be reformulated as a short-term average sum-rate (ASR) optimization for each channel estimate  $\hat{\mathbf{H}}_i^{\text{DD}}$ , expressed as

$$\mathcal{P}_1 : \max_{\mathbf{P}_{\text{BF}}, \Psi, \hat{\mathbf{c}}} \sum_{i=1}^I \hat{R}_{\text{tot},i}, \quad (26a)$$

$$\text{s.t.} \quad \sum_{i'=1}^I \hat{C}_{i'} \leq \hat{R}_{c,i}^{(L)}, \quad i \in \mathcal{I}, \quad (26b)$$

$$\text{tr}(\mathbf{P}_{\text{BF}} \mathbf{P}_{\text{BF}}^H) \leq P_t, \quad (26c)$$

$$\Psi_* \in \Psi, [\Psi_*]_{ij} = 0 \text{ for } i \neq j, [\Psi_*]_{ii} \in \{0, 1\}, \quad (26d)$$

$$\hat{\mathbf{c}} \geq \mathbf{0}, \quad (26e)$$

where  $\hat{\mathbf{c}} = [\hat{C}_1, \hat{C}_2, \dots, \hat{C}_I]$  denotes the vector of average common-rate allocations, and  $\hat{R}_{\text{tot},i} = \hat{C}_i + \hat{R}_{p,i}$  is the total average rate achieved by user  $i$ .

#### IV. PROPOSED ALGORITHM

The optimization problem in (26) is non-deterministic, making a direct solution intractable. To address this issue, we propose a three-stage procedure. First, the SAA method is used to obtain a deterministic approximation of the original statistical optimization problem. Second, the resultant ASR problem is reformulated as an average augmented weighted MSE (AWMSE) problem to efficiently address the rate maximization objective. Finally, vectorization transforms the AWMSE problem into a tractable formulation to avoid matrix inversion, whose sequential problem could finally be solved using AO.

##### A. Sample Average Approximation

Consider a set of  $L$  independent and identically distributed (i.i.d) channel realizations indexed by  $\mathcal{L} = \{1, 2, \dots, L\}$ , drawn from the conditional distribution with density  $f_{\mathbf{H}_i^{\text{DD}} | \hat{\mathbf{H}}_i^{\text{DD}}}(\mathbf{H}_i^{\text{DD}} | \hat{\mathbf{H}}_i^{\text{DD}})$ . For a specific estimated channel  $\hat{\mathbf{H}}_i^{\text{DD}}$ , the sampled channel is given by

$$\mathbb{H}_i^{\text{DD}(L)} \triangleq \left\{ \mathbf{H}_i^{\text{DD}(l)} = \hat{\mathbf{H}}_i^{\text{DD}} + \mathbf{E}_{h,i}^{(l)} \mid \hat{\mathbf{H}}_i^{\text{DD}}, l \in \mathcal{L} \right\}. \quad (27)$$

Based on the channel realizations, we define the sample average functions (SAFs) of the average rates as  $\hat{R}_{c,i}^{(L)} \triangleq \frac{1}{L} \sum_{l=1}^L R_{c,i}^{(l)}$ ,  $\hat{R}_{p,i}^{(L)} \triangleq \frac{1}{L} \sum_{l=1}^L R_{p,i}^{(l)}$ , where  $R_{z,i}^{(l)} \triangleq$

$R_{z,i}(\mathbf{H}_i^{\text{DD}(l)})$ ,  $z \in \{c, p\}$  represents the instantaneous common or private rate corresponding to the  $l$ -th channel realization.

The SAA formulation of the stochastic optimization problem (26) can thus be written as

$$\mathcal{P}_2 : \max_{\mathbf{P}_{\text{BF}}, \Psi, \hat{\mathbf{c}}} \sum_{i=1}^I \hat{R}_{\text{tot},i}^{(L)} \quad (28a)$$

$$\text{s.t.} \quad \sum_{i'=1}^I \hat{C}_{i'} \leq \hat{R}_{c,i}^{(L)}, \quad i \in \mathcal{I}, \quad (28b)$$

$$(26c), (26d), (26e), \quad (28c)$$

where  $\hat{R}_{\text{tot},i}^{(L)} = \hat{C}_i + \hat{R}_{p,i}^{(L)}$ . Since the achievable rates are bounded [28], the LLN ensures that

$$\lim_{L \rightarrow \infty} \hat{R}_{c,i}^{(L)}(\mathbf{P}_{\text{BF}}, \Psi) = \hat{R}_{c,i}(\mathbf{P}_{\text{BF}}, \Psi), \quad \forall \mathbf{P}_{\text{BF}} \in \mathbb{P}_{\text{BF}}, \Psi \in \mathbb{A}_{\text{M}} \quad (29a)$$

$$\lim_{L \rightarrow \infty} \hat{R}_{p,i}^{(L)}(\mathbf{P}_{\text{BF}}, \Psi) = \hat{R}_{p,i}(\mathbf{P}_{\text{BF}}, \Psi), \quad \forall \mathbf{P}_{\text{BF}} \in \mathbb{P}_{\text{BF}}, \Psi \in \mathbb{A}_{\text{M}}, \quad (29b)$$

where  $\mathbb{P}_{\text{BF}} \triangleq \{ \mathbf{P}_{\text{BF}} \in \mathbb{C}^{(I+1) \times N_t} \mid \text{tr}(\mathbf{P}_{\text{BF}} \mathbf{P}_{\text{BF}}^H) \leq P_t \}$  and  $\mathbb{A}_{\text{M}} \triangleq \{ \Psi_* \mid \Psi_* \in \Psi, [\Psi_*]_{ii} \in \{0, 1\}, [\Psi_*]_{ij} = 0 \text{ for } i \neq j \}$  denote the feasible set of precoders and arrangement matrices. Within these sets, the rate functions are bounded, continuous, and differentiable with respect to  $\mathbf{P}_{\text{BF}}$ , ensuring the convergence in (29). Therefore, as  $L \rightarrow \infty$ ,  $\hat{R}_{z,i}^{(L)}$  and  $\hat{R}_{z,i}$ ,  $z \in \{c, p\}$ , become asymptotically equivalent, leading to

$$\lim_{L \rightarrow \infty} \hat{R}_{\text{tot},i}^{(L)} = \hat{R}_{\text{tot},i}, \quad \forall \mathbf{P}_{\text{BF}} \in \mathbb{P}_{\text{BF}}, \Psi \in \mathbb{A}_{\text{M}}. \quad (30)$$

From (29) and (30), we obtain that the global optimal solution of the SAA problem in (28) converges to that of the original stochastic optimization problem in (26) as  $L \rightarrow \infty$  [28], [39]. We then proceed to solve the sampled problem in (28).

##### B. Average Augmented Weighted MSE Minimization

To efficiently solve the SAA problem in (28), we reformulate it into an equivalent AWMSE representation for tractability, following [40]. AWMSE formulations differ from conventional weighted MSE (WMSE) counterparts, since the weighted factors are treated as optimization variables rather than fixed parameters, and the objective function is modified to include the logarithmic terms of the weights. Then, the relationship between the achievable rate and the WMMSE is established based on the aforementioned features.

Let  $\mathbf{A}_{c,i}, \mathbf{A}_{p,i} \in \mathbb{C}^{MN \times MN}$  denote the receive equalizers (filters) for the common and private streams of user  $i$ , respectively. The estimated common stream is  $\hat{\mathbf{s}}_{c,i} = \mathbf{A}_{c,i} \mathbf{y}_i^{\text{DD}}$ . Once the common stream  $\mathbf{s}_c$  is successfully decoded and subtracted, the private stream of user  $i$  is estimated as  $\hat{\mathbf{s}}_{p,i} = \mathbf{A}_{p,i} (\mathbf{y}_i^{\text{DD}} - \mathbf{H}_i^{\text{DD}} \tilde{\mathbf{P}}_c \mathbf{s}_c)$ .

The mean square error (MSE) matrices of the common and private streams are expressed in (31a) and (31b) at the top of next page. The optimum MMSE equalizers are derived by minimizing the corresponding MSE expressions with respect

$$\mathbf{E}_{c,i} = \mathbb{E} \left\{ (\hat{\mathbf{s}}_{c,i} - \mathbf{s}_c)(\hat{\mathbf{s}}_{c,i} - \mathbf{s}_c)^H \right\} = \mathbf{A}_{c,i} \mathbf{y}_i^{\text{DD}} \mathbf{y}_i^{\text{DD}H} \mathbf{A}_{c,i}^H - \mathbf{A}_{c,i} \mathbf{y}_i^{\text{DD}} \mathbf{s}_c^H - \mathbf{s}_c \mathbf{y}_i^{\text{DD}H} \mathbf{A}_{c,i}^H + \mathbf{I}_{MN} \quad (31a)$$

$$\mathbf{E}_{p,i} = \mathbb{E} \left\{ (\hat{\mathbf{s}}_{p,i} - \mathbf{s}_{p,i})(\hat{\mathbf{s}}_{p,i} - \mathbf{s}_{p,i})^H \right\} = \mathbf{A}_{p,i} \mathbf{y}_i^{\text{DD}} \mathbf{y}_i^{\text{DD}H} \mathbf{A}_{p,i}^H - \mathbf{A}_{p,i} \mathbf{y}_i^{\text{DD}} \mathbf{s}_{p,i}^H - \mathbf{s}_{p,i} \mathbf{y}_i^{\text{DD}H} \mathbf{A}_{p,i}^H + \mathbf{I}_{MN} \quad (31b)$$

to the receive filters, i.e.,  $\frac{\partial \mathbf{E}_{c,i}}{\partial \mathbf{A}_{c,i}} = 0$ ,  $\frac{\partial \mathbf{E}_{p,i}}{\partial \mathbf{A}_{p,i}} = 0$ , which lead to

$$\begin{aligned} \mathbf{A}_{c,i}^{\text{MMSE}} &= \arg \min_{\mathbf{A}_{c,i}} \mathbb{E} \left\{ \|\mathbf{A}_{c,i} \mathbf{y}_i^{\text{DD}} - \mathbf{s}_c\|^2 \right\} \\ &= \tilde{\mathbf{P}}_c^H (\tilde{\mathbf{H}}_i^{\text{DD}})^H \mathbf{T}_{c,i}^{-1}, \end{aligned} \quad (32a)$$

$$\begin{aligned} \mathbf{A}_{p,i}^{\text{MMSE}} &= \arg \min_{\mathbf{A}_{p,i}} \mathbb{E} \left\{ \|\mathbf{A}_{p,i} \left( \mathbf{y}_i^{\text{DD}} - \tilde{\mathbf{H}}_i^{\text{DD}} \tilde{\mathbf{P}}_c \mathbf{s}_c \right) - \mathbf{s}_{p,i}\|^2 \right\} \\ &= \tilde{\mathbf{P}}_{p,i}^H (\tilde{\mathbf{H}}_i^{\text{DD}})^H \mathbf{T}_{p,i}^{-1}. \end{aligned} \quad (32b)$$

Substituting (32a) and (32b) into (31a) and (31b), respectively, the corresponding MMSE covariance matrices are obtained as

$$\mathbf{E}_{c,i}^{\text{MMSE}} \triangleq \min_{\mathbf{A}_{c,i}} \mathbf{E}_{c,i} = \left( \mathbf{I}_{MN} + \tilde{\mathbf{P}}_c^H (\tilde{\mathbf{H}}_i^{\text{DD}})^H \mathbf{K}_{c,i}^{-1} \tilde{\mathbf{H}}_i^{\text{DD}} \tilde{\mathbf{P}}_c \right)^{-1}, \quad (33a)$$

$$\mathbf{E}_{p,i}^{\text{MMSE}} \triangleq \min_{\mathbf{A}_{p,i}} \mathbf{E}_{p,i} = \left( \mathbf{I}_{MN} + \tilde{\mathbf{P}}_{p,i}^H (\tilde{\mathbf{H}}_i^{\text{DD}})^H \mathbf{K}_{p,i}^{-1} \tilde{\mathbf{H}}_i^{\text{DD}} \tilde{\mathbf{P}}_{p,i} \right)^{-1}. \quad (33b)$$

Accordingly, the instantaneous achievable rates are obtained as

$$R_{c,i} = \log_2 \det \left( \mathbf{E}_{c,i}^{\text{MMSE}} \right)^{-1}, \quad R_{p,i} = \log_2 \det \left( \mathbf{E}_{p,i}^{\text{MMSE}} \right)^{-1}. \quad (34)$$

By introducing weight matrices  $\mathbf{B}_{c,i}$  and  $\mathbf{B}_{p,i}$ , the AWMSE for decoding common and private streams at user- $i$  are expressed as

$$\xi_{c,i} = \text{tr} \left( \mathbf{B}_{c,i} \mathbf{E}_{c,i} \right) - \log \det \left( \mathbf{B}_{c,i} \right), \quad (35a)$$

$$\xi_{p,i} = \text{tr} \left( \mathbf{B}_{p,i} \mathbf{E}_{p,i} \right) - \log \det \left( \mathbf{B}_{p,i} \right). \quad (35b)$$

To establish the rate-WMMSE relationship, we treat the equalizers and weights as optimization variables. Taking the derivative of  $\xi_{c,i}$  and  $\xi_{p,i}$  with respect to  $\mathbf{A}_{c,i}$  and  $\mathbf{A}_{p,i}$  and setting the gradients to zero yields  $\frac{\partial \xi_{c,i}}{\partial \mathbf{A}_{c,i}} = 0$ ,  $\frac{\partial \xi_{p,i}}{\partial \mathbf{A}_{p,i}} = 0$ , which leads to the optimal equalizers

$$\mathbf{A}_{c,i}^* = \mathbf{A}_{c,i}^{\text{MMSE}}, \quad \mathbf{A}_{p,i}^* = \mathbf{A}_{p,i}^{\text{MMSE}}. \quad (36)$$

By substituting the MMSE equalizers into (35), the AWMSE can be rewritten as

$$\xi_{c,i}(\mathbf{A}_{c,i}^{\text{MMSE}}) = \text{tr} \left( \mathbf{B}_{c,i} \mathbf{E}_{c,i}^{\text{MMSE}} \right) - \log \det \left( \mathbf{B}_{c,i} \right), \quad (37a)$$

$$\xi_{p,i}(\mathbf{A}_{p,i}^{\text{MMSE}}) = \text{tr} \left( \mathbf{B}_{p,i} \mathbf{E}_{p,i}^{\text{MMSE}} \right) - \log \det \left( \mathbf{B}_{p,i} \right). \quad (37b)$$

Next, by differentiating  $\xi_{c,i}(\mathbf{A}_{c,i}^{\text{MMSE}})$  and  $\xi_{p,i}(\mathbf{A}_{p,i}^{\text{MMSE}})$  with respect to the corresponding weight matrix and setting the gradient to zero, i.e.,  $\frac{\partial \xi_{c,i}(\mathbf{A}_{c,i}^{\text{MMSE}})}{\partial \mathbf{B}_{c,i}} = 0$ ,  $\frac{\partial \xi_{p,i}(\mathbf{A}_{p,i}^{\text{MMSE}})}{\partial \mathbf{B}_{p,i}} = 0$ , the optimal MMSE weights are obtained as

$$\mathbf{B}_{c,i}^* = \mathbf{B}_{c,i}^{\text{MMSE}} \triangleq \left( \mathbf{E}_{c,i}^{\text{MMSE}} \right)^{-1}, \quad (38a)$$

$$\mathbf{B}_{p,i}^* = \mathbf{B}_{p,i}^{\text{MMSE}} \triangleq \left( \mathbf{E}_{p,i}^{\text{MMSE}} \right)^{-1}. \quad (38b)$$

Finally, substituting the optimal weights into (37) establishes the instantaneous rate-WMMSE relationships

$$\begin{aligned} \xi_{c,i} &\triangleq \min_{\mathbf{A}_{c,i}, \mathbf{B}_{c,i}} \xi_{c,i} = MN - R_{c,i}, \\ \xi_{p,i} &\triangleq \min_{\mathbf{A}_{p,i}, \mathbf{B}_{p,i}} \xi_{p,i} = MN - R_{p,i}. \end{aligned} \quad (39)$$

Following the SAA framework, the average rate-WMMSE relation is obtained by taking the expectation with respect to the conditional distribution of  $\mathbf{H}_i^{\text{DD}}$  given  $\hat{\mathbf{H}}_i^{\text{DD}}$ , leading to

$$\hat{\xi}_{c,i} \triangleq \mathbb{E}_{\mathbf{H}_i^{\text{DD}} | \hat{\mathbf{H}}_i^{\text{DD}}} \left\{ \min_{\mathbf{A}_{c,i}, \mathbf{B}_{c,i}} \xi_{c,i} \mid \hat{\mathbf{H}}_i^{\text{DD}} \right\} = MN - \hat{R}_{c,i}, \quad (40a)$$

$$\hat{\xi}_{p,i} \triangleq \mathbb{E}_{\mathbf{H}_i^{\text{DD}} | \hat{\mathbf{H}}_i^{\text{DD}}} \left\{ \min_{\mathbf{A}_{p,i}, \mathbf{B}_{p,i}} \xi_{p,i} \mid \hat{\mathbf{H}}_i^{\text{DD}} \right\} = MN - \hat{R}_{p,i}. \quad (40b)$$

To obtain deterministic counterparts of (40), the average AWMSEs are approximated using the SAFs method. Specifically,

$$\hat{\xi}_{c,i}^{(L)} \triangleq \frac{1}{L} \sum_{l=1}^L \xi_{c,i}^{(l)}, \quad \hat{\xi}_{p,i}^{(L)} \triangleq \frac{1}{L} \sum_{l=1}^L \xi_{p,i}^{(l)}, \quad (41)$$

where  $\xi_{c,i}^{(l)} \triangleq \xi_{c,i}(\mathbf{H}_i^{\text{DD}(l)}, \mathbf{A}_{c,i}^{(l)}, \mathbf{B}_{c,i}^{(l)})$ ,  $\xi_{p,i}^{(l)} \triangleq \xi_{p,i}(\mathbf{H}_i^{\text{DD}(l)}, \mathbf{A}_{p,i}^{(l)}, \mathbf{B}_{p,i}^{(l)})$ ,  $\mathbf{A}_{c,i}^{(l)} \triangleq \mathbf{A}_{c,i}(\mathbf{H}_i^{\text{DD}(l)})$ ,  $\mathbf{A}_{p,i}^{(l)} \triangleq \mathbf{A}_{p,i}(\mathbf{H}_i^{\text{DD}(l)})$ ,  $\mathbf{B}_{c,i}^{(l)} \triangleq \mathbf{B}_{c,i}(\mathbf{H}_i^{\text{DD}(l)})$ , and  $\mathbf{B}_{p,i}^{(l)} \triangleq \mathbf{B}_{p,i}(\mathbf{H}_i^{\text{DD}(l)})$  all correspond to the  $l$ -th realization in  $\mathbb{H}_i^{\text{DD}(L)}$ . For notational convenience, we define  $\mathbf{A} \triangleq \{\mathbf{A}_{c,i}^{\mathcal{L}}, \mathbf{A}_{p,i}^{\mathcal{L}} \mid i \in \mathcal{I}\}$ , where  $\mathbf{A}_{c,i}^{\mathcal{L}} \triangleq \{\mathbf{A}_{c,i}^{(l)} \mid l \in \mathcal{L}\}$  and  $\mathbf{A}_{p,i}^{\mathcal{L}} \triangleq \{\mathbf{A}_{p,i}^{(l)} \mid l \in \mathcal{L}\}$ . Similarly, we define  $\mathbf{B} \triangleq \{\mathbf{B}_{c,i}^{\mathcal{L}}, \mathbf{B}_{p,i}^{\mathcal{L}} \mid i \in \mathcal{I}\}$ , where  $\mathbf{B}_{c,i}^{\mathcal{L}} \triangleq \{\mathbf{B}_{c,i}^{(l)} \mid l \in \mathcal{L}\}$  and  $\mathbf{B}_{p,i}^{\mathcal{L}} \triangleq \{\mathbf{B}_{p,i}^{(l)} \mid l \in \mathcal{L}\}$ . Adopting the same approach as that utilized in proving (39), the average rate-WMMSE can be written as

$$\left( \hat{\xi}_{c,i}^{\text{MMSE}} \right)^{(L)} \triangleq \min_{\mathbf{A}_{c,i}, \mathbf{B}_{c,i}} \hat{\xi}_{c,i}^{(L)} = MN - \hat{R}_{c,i}^{(L)}, \quad (42a)$$

$$\left( \hat{\xi}_{p,i}^{\text{MMSE}} \right)^{(L)} \triangleq \min_{\mathbf{A}_{p,i}, \mathbf{B}_{p,i}} \hat{\xi}_{p,i}^{(L)} = MN - \hat{R}_{p,i}^{(L)}. \quad (42b)$$

The set of optimal MMSE equalizer corresponding to (42) are expressed as  $\mathbf{A}_{c,i}^{\text{MMSE}} \triangleq \{\mathbf{A}_{c,i}^{\text{MMSE}(l)} \mid l \in \mathcal{L}\}$ ,  $\mathbf{A}_{p,i}^{\text{MMSE}} \triangleq \{\mathbf{A}_{p,i}^{\text{MMSE}(l)} \mid l \in \mathcal{L}\}$ . Similarly, the set of corresponding optimal MMSE weight matrices are defined as  $\mathbf{B}_{c,i}^{\text{MMSE}} \triangleq \{\mathbf{B}_{c,i}^{\text{MMSE}(l)} \mid l \in \mathcal{L}\}$ ,  $\mathbf{B}_{p,i}^{\text{MMSE}} \triangleq \{\mathbf{B}_{p,i}^{\text{MMSE}(l)} \mid l \in \mathcal{L}\}$ . By aggregating all  $I$  users, the MMSE equalizer and weight collections are given by  $\mathbf{A}^{\text{MMSE}} \triangleq \{\mathbf{A}_{c,i}^{\text{MMSE}}, \mathbf{A}_{p,i}^{\text{MMSE}} \mid i \in \mathcal{I}\}$ ,  $\mathbf{B}^{\text{MMSE}} \triangleq \{\mathbf{B}_{c,i}^{\text{MMSE}}, \mathbf{B}_{p,i}^{\text{MMSE}} \mid i \in \mathcal{I}\}$ . Building upon

the relationship established in (42), the deterministic average AWMSE minimization problem is formulated as

$$\mathcal{P}_3 : \min_{\substack{\mathbf{P}_{\text{BF}}, \Psi, \\ \hat{\boldsymbol{\mu}}, \mathbf{A}, \mathbf{B}}} \sum_{i=1}^I \hat{\xi}_{\text{tot},i}^{(L)} \quad (43a)$$

$$\text{s.t.} \quad \sum_{i=1}^I \hat{\mu}_i + MN \geq \hat{\xi}_{c,i}^{(L)}, \quad i \in \mathcal{I} \quad (43b)$$

$$\hat{\boldsymbol{\mu}} \leq \mathbf{0}, \quad (43c)$$

$$(26c), (26d), \quad (43d)$$

where  $\hat{\xi}_{\text{tot},i}^{(L)} = \hat{\mu}_i + \hat{\xi}_{p,i}^{(L)}$  and  $\hat{\boldsymbol{\mu}} = [\hat{\mu}_1, \hat{\mu}_2, \dots, \hat{\mu}_I] = -\hat{\mathbf{c}}$ . The optimization in (43) with respect to  $(\mathbf{A}, \mathbf{B})$  is obtained by minimizing the individual average AWMSE in (42), as the average AWMSEs are decoupled with respect to their corresponding equalizers and weights. This can be verified by showing that the Karush-Kuhn-Tucker (KKT) optimality conditions of (43) are satisfied for a given precoder  $\mathbf{P}_{\text{BF}}$  and arrangement set  $\Psi$  when  $\{\mathbf{A}, \mathbf{B}\} = \{\mathbf{A}^{\text{MMSE}}, \mathbf{B}^{\text{MMSE}}\}$ . Under this setting, problem (43) simplifies to (28), demonstrating that the rate-WMMSE equivalence holds not only at the global optimum but also at all stationary points. Furthermore, any feasible points  $\{\mathbf{A}^*, \mathbf{B}^*, \mathbf{P}_{\text{BF}}^*, \Psi^*, \hat{\boldsymbol{\mu}}^*\}$  satisfying the KKT conditions of (43) also satisfies those of (28) with  $\hat{\boldsymbol{\mu}} = -\hat{\mathbf{c}}$  [28]. Consequently, as  $L \rightarrow \infty$ , the optimal solution of (43) converges to that of (28), which in turn corresponds to the solution of the ASR problem in (26).

### C. Vectorization

Unlike the SISO scenario considered in [25], [27], [41], the matrix variables in (43) makes the optimization process challenging. Specifically, solving (43) requires managing  $\hat{\xi}_{\text{tot},i}^{(L)}$  in (43a) and  $\hat{\xi}_{c,i}^{(L)}$  in (43b), which are linear combinations with the instantaneous AWMSE expressions  $\xi_{\text{tot},i}^{(l)}$  and  $\xi_{c,i}^{(l)}$  in (37). Unfortunately, the optimal solution of (37), based on (38), necessitates calculating the matrix inversions,  $\mathbf{K}_{c,i}^{-1}$  and  $\mathbf{K}_{p,i}^{-1}$ , as shown in (33). This ultimately introduces significant computational complexity and hinders the problem's convexity.

To avoid matrix inversion, we do not optimize the precoder directly using (38). Instead, we revert to the instantaneous AWMSE expressions  $\xi_{\text{tot},i}^{(l)}$  and  $\xi_{c,i}^{(l)}$  in (37), and expand its main components  $\text{tr}(\mathbf{B}_{c,i} \mathbf{E}_{c,i})$  as in (44) at the top of next page. After algebraic simplification, we obtain the whole expression of  $\xi_{\text{tot},i}^{(l)}$  and  $\xi_{c,i}^{(l)}$  from (37) in (45a), where  $\tilde{\mathbf{p}}_c \triangleq \text{vec}(\tilde{\mathbf{P}}_c)$ , and  $\tilde{\mathbf{p}}_{p,i} \triangleq \text{vec}(\tilde{\mathbf{P}}_{p,i})$  for  $i \in \mathcal{I}$ . Similarly, the corresponding formulation for  $\text{tr}(\mathbf{B}_{p,i} \mathbf{E}_{p,i}) - \log \det(\mathbf{B}_{p,i})$  from (37) is derived in (45b).

However, the expressions in (45) are cumbersome. Closer inspection reveals that the third and fourth terms,  $t_3$  and  $t_4$ , in (45a) are inherently connected, and the same observation holds for the corresponding terms in (45b). We further establish that the weight matrices  $\mathbf{B}_{c,i}$  and  $\mathbf{B}_{p,i}$  are Hermitian when taking the optimal values, that is,  $\mathbf{B}_{c,i}^{\text{MMSE}} = (\mathbf{B}_{c,i}^{\text{MMSE}})^H$  and  $\mathbf{B}_{p,i}^{\text{MMSE}} = (\mathbf{B}_{p,i}^{\text{MMSE}})^H$ . These properties enable (45a) and

(45b) to be simplified and expressed in compact forms, as shown in (46a) and (46b) at the top of next page, where

$$\mathbf{C}_{c,i} = \mathbf{I}_{MN} \otimes (\tilde{\mathbf{H}}_i^{\text{DD}})^H \mathbf{A}_{c,i}^H \mathbf{B}_{c,i} \mathbf{A}_{c,i} \tilde{\mathbf{H}}_i^{\text{DD}},$$

$$\mathbf{C}_{p,i} = \mathbf{I}_{MN} \otimes (\tilde{\mathbf{H}}_i^{\text{DD}})^H \mathbf{A}_{p,i}^H \mathbf{B}_{p,i} \mathbf{A}_{p,i} \tilde{\mathbf{H}}_i^{\text{DD}},$$

$$\mathbf{d}_{c,i} = \text{vec}((\tilde{\mathbf{H}}_i^{\text{DD}})^H \mathbf{A}_{c,i}^H \mathbf{B}_{c,i}), \quad \mathbf{d}_{p,i} = \text{vec}((\tilde{\mathbf{H}}_i^{\text{DD}})^H \mathbf{A}_{p,i}^H \mathbf{B}_{p,i}),$$

$$d_{c,i} = \sigma_{n,i}^2 \text{tr}(\mathbf{B}_{c,i} \mathbf{A}_{c,i} \mathbf{A}_{c,i}^H) + \text{tr}(\mathbf{B}_{c,i}) - \log \det(\mathbf{B}_{c,i}),$$

$$d_{p,i} = \sigma_{n,i}^2 \text{tr}(\mathbf{B}_{p,i} \mathbf{A}_{p,i} \mathbf{A}_{p,i}^H) + \text{tr}(\mathbf{B}_{p,i}) - \log \det(\mathbf{B}_{p,i}).$$

### D. Alternating Optimization

Problem (43) is inherently non-convex when jointly optimizing the variables  $\mathbf{A}$ ,  $\mathbf{B}$ ,  $\mathbf{P}_{\text{BF}}$ ,  $\Psi$  and  $\hat{\boldsymbol{\mu}}$ . However, it becomes convex with respect to each variable block when the remaining ones are fixed. Therefore, an AO strategy is adopted, consisting of three main steps: (1) The equalizers  $\mathbf{A}$  and weights  $\mathbf{B}$  are updated while keeping the precoder  $\mathbf{P}_{\text{BF}}$  and the arrangement matrix set  $\Psi$  fixed. (2) The precoder  $\mathbf{P}_{\text{BF}}$  and message split  $\hat{\boldsymbol{\mu}}$  are optimized for the fixed  $\Psi$  and the updated  $\mathbf{A}$  and  $\mathbf{B}$ . (3) The arrangement matrix set  $\Psi$  is then updated based on the updated  $\mathbf{P}_{\text{BF}}$ ,  $\mathbf{A}$ , and  $\mathbf{B}$ .

- 1) *Update equalizers and weights.* For each channel realization, in the  $k$ -th iteration of the AO algorithm, the equalizers and weights are updated according to

$$(\mathbf{A}, \mathbf{B}) = (\mathbf{A}^{\text{MMSE}}(\mathbf{X}^{[k-1]}), \mathbf{B}^{\text{MMSE}}(\mathbf{X}^{[k-1]})), \quad (47)$$

where  $\mathbf{X}^{[k-1]} \triangleq (\mathbf{P}_{\text{BF}}^{[k-1]}, \Psi^{[k-1]})$ , therein,  $\mathbf{P}_{\text{BF}}^{[k-1]}$  and  $\Psi^{[k-1]}$  are the precoding and arrangement matrices obtained from the  $(k-1)$ -th iteration. To facilitate the subsequent optimization of  $\mathbf{P}_{\text{BF}}$ , we define a set of SAFs as  $\{\hat{\mathbf{C}}_{c,i}, \hat{\mathbf{C}}_{p,i}, \hat{\mathbf{d}}_{c,i}, \hat{\mathbf{d}}_{p,i}, \hat{d}_{c,i}, \hat{d}_{p,i}\}$ , which are computed based on the updated  $(\mathbf{A}, \mathbf{B})$ . Specifically, they are defined as the ensemble means of their instantaneous values:

$$\hat{\mathbf{C}}_{c,i} = \frac{1}{L} \sum_{l=1}^L \mathbf{C}_{c,i}^{(l)}, \quad \hat{\mathbf{d}}_{c,i} = \frac{1}{L} \sum_{l=1}^L \mathbf{d}_{c,i}^{(l)}, \quad \hat{d}_{c,i} = \frac{1}{L} \sum_{l=1}^L d_{c,i}^{(l)},$$

$$\hat{\mathbf{C}}_{p,i} = \frac{1}{L} \sum_{l=1}^L \mathbf{C}_{p,i}^{(l)}, \quad \hat{\mathbf{d}}_{p,i} = \frac{1}{L} \sum_{l=1}^L \mathbf{d}_{p,i}^{(l)}, \quad \hat{d}_{p,i} = \frac{1}{L} \sum_{l=1}^L d_{p,i}^{(l)}.$$

- 2) *Update precoders.* Given the arrangement matrix set and the updated equalizers and weights, the precoder update problem is formulated by substituting  $\mathbf{A}^{\text{MMSE}}(\mathbf{X}^{[k-1]})$ ,  $\mathbf{B}^{\text{MMSE}}(\mathbf{X}^{[k-1]})$  and SAFs set of dependent entities into (43), leading to

$$\mathcal{P}_4 : \min_{\mathbf{P}_{\text{BF}}, \hat{\boldsymbol{\mu}}} t \quad (48a)$$

$$\text{s.t.} \quad \sum_{i=1}^I (\hat{\mu}_i + \hat{\phi}_{p,i}) - t \leq 0, \quad (48b)$$

$$\hat{\phi}_{c,i} - \sum_{i'=1}^I \hat{\mu}_{i'} - MN \leq 0, \quad i \in \mathcal{I} \quad (48c)$$

$$(26c), (26d), (43c), \quad (48d)$$

$$\begin{aligned}
\text{tr} \{ \mathbf{B}_{c,i} \mathbf{E}_{c,i} \} &= \text{tr} \left\{ \mathbf{B}_{c,i} \mathbb{E} \left[ (\mathbf{A}_{c,i} \mathbf{y}_i^{\text{DD}} - \mathbf{s}_c) (\mathbf{A}_{c,i} \mathbf{y}_i^{\text{DD}} - \mathbf{s}_c)^H \right] \right\} \\
&= \text{tr} \left\{ \mathbf{B}_{c,i} \mathbf{A}_{c,i} \tilde{\mathbf{H}}_i^{\text{DD}} \tilde{\mathbf{P}}_c \tilde{\mathbf{P}}_c^H (\tilde{\mathbf{H}}_i^{\text{DD}})^H \mathbf{A}_{c,i}^H + \mathbf{B}_{c,i} \mathbf{A}_{c,i} \sum_{i'=1}^I \tilde{\mathbf{H}}_i^{\text{DD}} \tilde{\mathbf{P}}_{p,i'} \tilde{\mathbf{P}}_{p,i'}^H (\tilde{\mathbf{H}}_i^{\text{DD}})^H \mathbf{A}_{c,i}^H \right. \\
&\quad \left. - \mathbf{B}_{c,i} \mathbf{A}_{c,i} \tilde{\mathbf{H}}_i^{\text{DD}} \tilde{\mathbf{P}}_c - \mathbf{B}_{c,i} \tilde{\mathbf{P}}_c^H (\tilde{\mathbf{H}}_i^{\text{DD}})^H \mathbf{A}_{c,i}^H + \sigma_{n,i}^2 \mathbf{B}_{c,i} \mathbf{A}_{c,i} \mathbf{A}_{c,i}^H + \mathbf{B}_{c,i} \mathbf{I}_{MN} \right\}. \tag{44}
\end{aligned}$$

$$\begin{aligned}
\text{tr}(\mathbf{B}_{c,i} \mathbf{E}_{c,i}) - \log \det(\mathbf{B}_{c,i}) &= \tilde{\mathbf{p}}_c^H \left[ \mathbf{I}_{MN} \otimes (\tilde{\mathbf{H}}_i^{\text{DD}})^H \mathbf{A}_{c,i}^H \mathbf{B}_{c,i} \mathbf{A}_{c,i} \tilde{\mathbf{H}}_i^{\text{DD}} \right] \tilde{\mathbf{p}}_c + \sum_{i'=1}^I \tilde{\mathbf{p}}_{p,i'}^H \left[ \mathbf{I}_{MN} \otimes (\tilde{\mathbf{H}}_i^{\text{DD}})^H \mathbf{A}_{c,i}^H \mathbf{B}_{c,i} \mathbf{A}_{c,i} \tilde{\mathbf{H}}_i^{\text{DD}} \right] \tilde{\mathbf{p}}_{p,i'} \\
&\quad - \underbrace{\left[ \text{vec} \left( (\tilde{\mathbf{H}}_i^{\text{DD}})^H \mathbf{A}_{c,i}^H \mathbf{B}_{c,i} \right) \right]^H}_{l_3} \tilde{\mathbf{p}}_c - \underbrace{\tilde{\mathbf{p}}_c^H \text{vec} \left( (\tilde{\mathbf{H}}_i^{\text{DD}})^H \mathbf{A}_{c,i}^H \mathbf{B}_{c,i} \right)}_{l_4} + \sigma_{n,i}^2 \text{tr}(\mathbf{B}_{c,i} \mathbf{A}_{c,i} \mathbf{A}_{c,i}^H) + \text{tr}(\mathbf{B}_{c,i}) - \log \det(\mathbf{B}_{c,i}), \tag{45a}
\end{aligned}$$

$$\begin{aligned}
\text{tr}(\mathbf{B}_{p,i} \mathbf{E}_{p,i}) - \log \det(\mathbf{B}_{p,i}) &= \tilde{\mathbf{p}}_{p,i}^H \left[ \mathbf{I}_{MN} \otimes (\tilde{\mathbf{H}}_i^{\text{DD}})^H \mathbf{A}_{p,i}^H \mathbf{B}_{p,i} \mathbf{A}_{p,i} \tilde{\mathbf{H}}_i^{\text{DD}} \right] \tilde{\mathbf{p}}_{p,i} + \sum_{i' \neq i} \tilde{\mathbf{p}}_{p,i'}^H \left[ \mathbf{I}_{MN} \otimes (\tilde{\mathbf{H}}_i^{\text{DD}})^H \mathbf{A}_{p,i}^H \mathbf{B}_{p,i} \mathbf{A}_{p,i} \tilde{\mathbf{H}}_i^{\text{DD}} \right] \tilde{\mathbf{p}}_{p,i'} \\
&\quad - \left[ \text{vec} \left( (\tilde{\mathbf{H}}_i^{\text{DD}})^H \mathbf{A}_{p,i}^H \mathbf{B}_{p,i} \right) \right]^H \tilde{\mathbf{p}}_{p,i} - \tilde{\mathbf{p}}_{p,i}^H \text{vec} \left( (\tilde{\mathbf{H}}_i^{\text{DD}})^H \mathbf{A}_{p,i}^H \mathbf{B}_{p,i} \right) + \sigma_{n,i}^2 \text{tr}(\mathbf{B}_{p,i} \mathbf{A}_{p,i} \mathbf{A}_{p,i}^H) + \text{tr}(\mathbf{B}_{p,i}) - \log \det(\mathbf{B}_{p,i}), \tag{45b}
\end{aligned}$$

$$\begin{aligned}
\text{tr}(\mathbf{B}_{c,i} \mathbf{E}_{c,i}) - \log \det(\mathbf{B}_{c,i}) &= \tilde{\mathbf{p}}_c^H \mathbf{C}_{c,i} \tilde{\mathbf{p}}_c + \sum_{i'=1}^I \tilde{\mathbf{p}}_{p,i'}^H \mathbf{C}_{c,i} \tilde{\mathbf{p}}_{p,i'} - \mathbf{d}_{c,i}^H \tilde{\mathbf{p}}_c - \tilde{\mathbf{p}}_c^H \mathbf{d}_{c,i} + d_{c,i} \\
&= \tilde{\mathbf{p}}_c^H \mathbf{C}_{c,i} \tilde{\mathbf{p}}_c + \sum_{i'=1}^I \tilde{\mathbf{p}}_{p,i'}^H \mathbf{C}_{c,i} \tilde{\mathbf{p}}_{p,i'} - 2\text{Re} \{ \mathbf{d}_{c,i}^H \tilde{\mathbf{p}}_c \} + d_{c,i}, \tag{46a}
\end{aligned}$$

$$\text{tr}(\mathbf{B}_{p,i} \mathbf{E}_{p,i}) - \log \det(\mathbf{B}_{p,i}) = \tilde{\mathbf{p}}_{p,i}^H \mathbf{C}_{p,i} \tilde{\mathbf{p}}_{p,i} + \sum_{i' \neq i} \tilde{\mathbf{p}}_{p,i'}^H \mathbf{C}_{p,i} \tilde{\mathbf{p}}_{p,i'} - 2\text{Re} \{ \mathbf{d}_{p,i}^H \tilde{\mathbf{p}}_{p,i} \} + d_{p,i}. \tag{46b}$$

where  $\hat{\phi}_{c,i} = \tilde{\mathbf{p}}_c^H \hat{\mathbf{C}}_{c,i} \tilde{\mathbf{p}}_c + \sum_{i'=1}^I \tilde{\mathbf{p}}_{p,i'}^H \hat{\mathbf{C}}_{c,i} \tilde{\mathbf{p}}_{p,i'} - 2\text{Re} \{ \hat{\mathbf{d}}_{c,i}^H \tilde{\mathbf{p}}_c \} + \hat{d}_{c,i}$  and  $\hat{\phi}_{p,i} = \tilde{\mathbf{p}}_{p,i}^H \hat{\mathbf{C}}_{p,i} \tilde{\mathbf{p}}_{p,i} + \sum_{i' \neq i} \tilde{\mathbf{p}}_{p,i'}^H \hat{\mathbf{C}}_{p,i} \tilde{\mathbf{p}}_{p,i'} - 2\text{Re} \{ \hat{\mathbf{d}}_{p,i}^H \tilde{\mathbf{p}}_{p,i} \} + \hat{d}_{p,i}$ . Problem (48) constitutes a convex quadratically constrained quadratic program (QCQP), which can be efficiently solved via interior-point methods [42], [43].

3) *Update arrangement matrices.* Given the updated equalizers, weights, and precoder, the arrangement matrices update problem is formulated by substituting  $\mathbf{P}_{\text{BF}}^{[k]}$  into (48), leading to

$$\mathcal{P}_5 : \min_{\Psi} t \tag{49a}$$

$$\text{s.t.} \quad (48b), (48c), (26c), (26d), (43c). \tag{49b}$$

Problem (49) constitutes a mixed-integer problem, which can be solved via MOSEK optimization toolbox [44].

The three steps are alternately executed until convergence, as summarized in Algorithm 1, where  $\epsilon$  denotes an arbitrarily small threshold. The problems (48) and (49) are solved by CVX toolbox in Matlab [44], [45]. For a given sample set  $\mathbb{H}_i^{\text{DD}(L)}$ , the sequence of optimized variables generated by Algorithm 1 converges to the set of KKT points of the corresponding sampled ASR problem in (28). Furthermore, as  $L \rightarrow \infty$ , the iterates converge almost surely to the set of KKT solutions of the original ASR problem in (26) [28].

---

#### Algorithm 1: Alternating Optimization algorithm

---

- 1 **Initialize:**  $k = 0$ ,  $\mathbf{P}_{\text{BF}}^{[0]}$ ;
  - 2 **repeat**
  - 3      $k \leftarrow k + 1$ ;
  - 4      $\mathbf{A} = \mathbf{A}^{\text{MMSE}}(\mathbf{P}_{\text{BF}}^{[k-1]})$ ,  $\mathbf{B} = \mathbf{B}^{\text{MMSE}}(\mathbf{P}_{\text{BF}}^{[k-1]})$ ;
  - 5     Compute  $\hat{\mathbf{C}}_{c,i}$ ,  $\hat{\mathbf{C}}_{p,i}$ ,  $\hat{\mathbf{d}}_{c,i}$ ,  $\hat{\mathbf{d}}_{p,i}$ ,  $\hat{d}_{c,i}$ ,  $\hat{d}_{p,i}$ ,  $\forall i \in \mathcal{I}$ ;
  - 6     Solve problem (48) and denote the optimal solutions as  $\mathbf{P}_{\text{BF}}^*$ ,  $\hat{\boldsymbol{\mu}}^*$ ;
  - 7     Solve problem (49) and denote the optimal value of the objective function as  $t^*$  and the optimal solutions as  $\Psi^*$ ;
  - 8     Update  $t^{[k]} \leftarrow t^*$ ,  $\mathbf{P}_{\text{BF}}^{[k]} \leftarrow \mathbf{P}_{\text{BF}}^*$ ,  $\hat{\boldsymbol{\mu}}^{[k]} \leftarrow \hat{\boldsymbol{\mu}}^*$ ,  $\Psi^{[k]} \leftarrow \Psi^*$ ;
  - 9 **until**  $t^{[k]} - t^{[k-1]} < \epsilon$ ;
- 

## V. SIMULATION RESULTS

In this section, we evaluate the performance of the proposed RSMA-OTFS scheme. The performance of the proposed scheme is compared with the following baseline schemes. SDMA-OTFS: A conventional SDMA scheme where each user's data is transmitted independently using OTFS modulation, i.e., no power is allocated to common streams. NOMA-OTFS: In a  $I$ -user NOMA scheme,  $i$ -th user message is

TABLE I: Simulation Parameters

Parameters	Values
LEO satellite altitude	500 km
LEO satellite velocity	$7.58 \times 10^3$ m/s
Carrier frequency	7.6 GHz
Subcarrier spacing	480 kHz
Bandwidth	128.88 MHz
Number of NLoS paths	2
Rician factor	10 dB
AoD range	$\theta_{i,q} \in [-\frac{\pi}{2}, \frac{\pi}{2})$
NLoS channel gain variance	$\sigma_{i,q}^2 = 1$
SNR of the pilot signal	$\gamma_e = 30$ dB
Channel error samples	$L = 1000$

decoded after  $i - 1$  user's signal are removed. We assume that the user with higher channel gain decodes and removes the interference from the user with lower channel gain before decoding its own signal. Specifically, for 2-user case, NOMA is a particular instance of RSMA, i.e., no power is allocated to one private stream and the entire common stream is utilized to transmit the message of a single user [17], [29]. The simulation setup is summarized in Table I. The performance metric used in the simulations is the ESR, which is averaged over 100 random channel realizations.

First, Fig. 3 illustrates the performance loss that arises with fractional delay and Doppler shifts, as well as the with the practical non-ideal rectangular pulse shaping. The curve labeled "Ideal (perfect) RSMA-OTFS" corresponds to a system model that does not incorporate these impairments, whereas "Non-ideal RSMA-OTFS" evaluates the performance under realistic conditions using the optimized precoders of the idealized model. A substantial degradation is observed when the impairments are omitted, and the loss becomes more pronounced in high SNR regimes. The curves "Non-ideal (perfect) RSMA-OTFS" and "Non-ideal (imperfect) RSMA-OTFS" represent the cases with perfect and imperfect CSIT, respectively, under realistic conditions. The proposed RSMA-OTFS approach, under both perfect and imperfect CSIT, achieves substantial performance gains over conventional RSMA-OFDM modulation in high-mobility scenarios. Notably, the performance of "Non-ideal RSMA-OTFS" falls below that of "Non-ideal (imperfect) RSMA-OTFS", indicating that the combined impact of fractional delay, Doppler shifts, and rectangular pulse shaping is more severe than that of imperfect CSIT. These observations demonstrate the necessity of evaluating and optimizing system performance under realistic conditions in OTFS-based systems.

The impact of imperfect CSIT is illustrated in Fig. 4a and Fig. 4b. The results show that RSMA-OTFS achieves higher ESR than SDMA-OTFS and NOMA-OTFS under both perfect and imperfect CSIT. All schemes experience performance degradation when the CSIT quality decreases, yet the reduction is more significant for the SDMA-OTFS scheme and Fig. 4a shows the DoF loss incurred by NOMA-OTFS as predicted in [16]. This behavior confirms that RSMA-

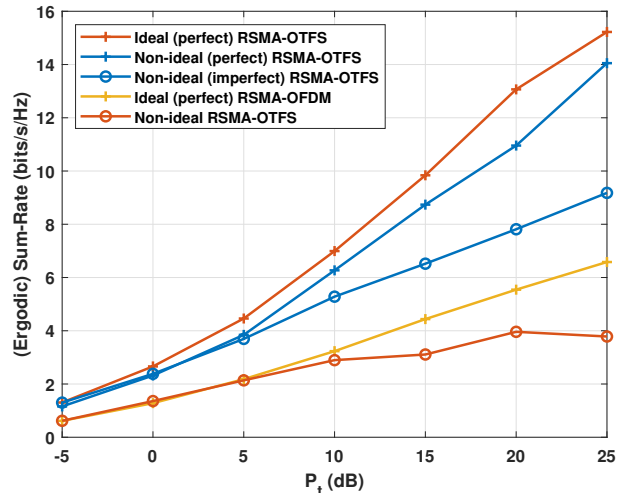


Fig. 3. Ergodic sum-rate comparison of different strategies with/without fractional Delay, Doppler Shift and rectangular pulse shaping effects,  $M = N = 4$ ,  $N_t = 2$ ,  $I = 2$ ,  $\rho = 0.7$ .

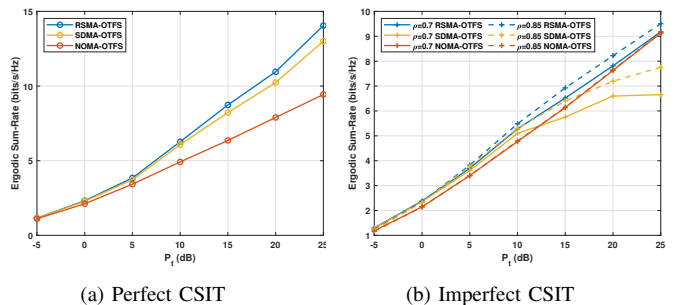


Fig. 4. Ergodic sum-rate comparison of different strategies under perfect and imperfect CSIT conditions,  $M = N = 4$ ,  $N_t = 2$ ,  $I = 2$ .

OTFS is intrinsically more resilient to CSIT imperfections because the common stream provides additional flexibility for interference mitigation. Although NOMA-OTFS exhibits a similar trend, the performance gap between perfect and imperfect CSIT remains smaller, since NOMA does not fully benefit from accurate CSIT. The influence of varying CSIT quality is further examined in Fig. 4b. As the channel correlation coefficient  $\rho$  decreases, indicating more severe CSIT imperfections, all schemes experience a decline in ESR. The reduction stems from the limited accuracy in precoding and interference management when CSIT deteriorates. Notably, the relative gain<sup>3</sup> of RSMA-OTFS over SDMA-OTFS increases from 12.49% to 15.54% when  $\rho$  decreases from 0.85 to 0.7 at  $P_t = 20$  dB, which confirms that RSMA-OTFS retains its advantage even as the CSIT quality worsens. Across all CSIT conditions, the proposed RSMA-OTFS scheme maintains superior performance, demonstrating its suitability for multi-user multi-antenna systems with imperfect or partial CSIT.

Next, the impact of OTFS frame resources on the system performance is evaluated and shown in Fig. 5. The notations "M4N4 RSMA-OTFS", and "M8N8 RSMA-OTFS" represent the proposed RSMA-OTFS scheme with OTFS frame config-

<sup>3</sup>The relative gain between two schemes  $x$  and  $y$  is defined as  $(x - y)/x$ .

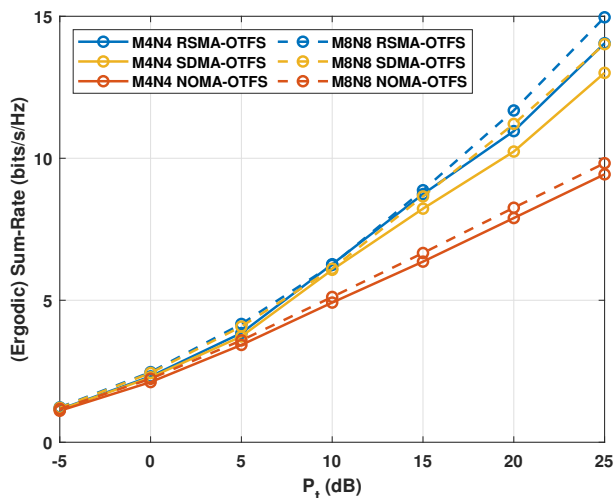


Fig. 5. Sum-rate comparison of different strategies with different OTFS frame resources,  $N_t = 2$ ,  $I = 2$ ,  $\rho = 0.7$ .

urations of  $M = 4$ ,  $N = 4$  and  $M = 8$ ,  $N = 8$ , respectively. Similar notations are used for the baseline schemes. It can be observed that increasing the number of subcarriers  $M$  and the number of time slots  $N$  leads to performance improvement in the ESR performance for all schemes. This is because larger OTFS frame resources enhance the delay and Doppler resolution for channel estimation, hence reducing the effect of fractional delay and Doppler shift, which enhances the overall system performance. Additionally, it is evident that the proposed RSMA-OTFS scheme consistently outperforms the baseline schemes across different OTFS frame configurations, demonstrating its effectiveness in leveraging the available resources.

Fig. 6a and Fig. 6b present the performance comparison under underloaded and overloaded user deployments. In the underloaded setting, the number of transmit antennas is greater than or equal to the number of users, whereas in the overloaded setting the number of users exceeds the number of transmit antennas. Across both scenarios, the proposed RSMA-OTFS scheme achieves higher performance than the SDMA-OTFS and NOMA-OTFS baselines. The figures further show that when the system transitions from the underloaded case ( $I = 2$ ) to the overloaded case ( $I = 4$ ), the relative rate gain of RSMA-OTFS over SDMA-OTFS decreases from 6.56% to 4.83% under perfect CSIT, and from 15.50% to 11.97% under imperfect CSIT, with  $P_t = 20$  dB. This indicates that RSMA-OTFS remains effective in both scenarios, and the gain is more evident when the transmitter has imperfect channel knowledge. As the number of users increases, the relative gain becomes smaller because both RSMA and SDMA may deactivate one private stream when the number of users exceeds the number of transmit antennas, which reduces the performance gap. In addition, the contribution of the common stream to the overall multiplexing gain becomes less influential compared with that of the private streams. The results demonstrate that the proposed RSMA-OTFS scheme consistently outperforms the SDMA-OTFS and NOMA-OTFS baselines across different

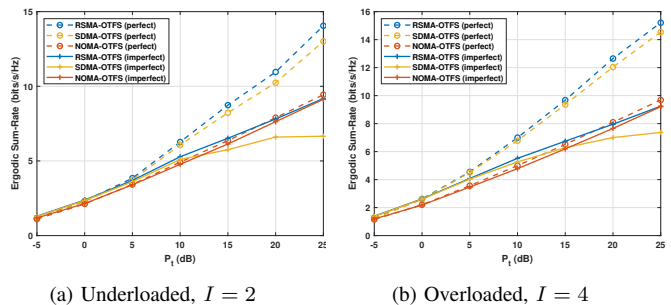


Fig. 6. Ergodic sum-rate comparison of different strategies with underloaded and overloaded deployments,  $M = N = 4$ ,  $N_t = 2$ .

user deployment configurations.

## VI. CONCLUSION

This work investigated the integration of RSMA and OTFS for downlink multi-user multi-antenna transmission in LEO satellite systems, where rapid channel variations and imperfect CSIT pose significant challenges. A robust transmission framework was developed to account for practical propagation effects, including rectangular pulse shaping, fractional Doppler shifts, fractional delays, and statistical CSIT. Within this framework, a compact cross-domain input-output relationship was derived, enabling a tractable problem optimization. Based on the proposed model, an ESR maximization problem was formulated by jointly optimizing the precoders, message splitting, power allocation, and precoder arrangement. The resulting non-convex problem was solved using a WMMSE-based AO algorithm that does not rely on sparsity assumptions of the DD-domain channel. Numerical results showed that ignoring practical impairments can lead to severe performance degradation, while the proposed multi-antenna RSMA-OTFS scheme consistently achieves higher ESR and improved robustness to CSIT uncertainty across various channel conditions and user deployments. These results highlight the effectiveness of the proposed framework and its potential for future LEO satellite communication systems.

## REFERENCES

- [1] 3GPP TR 38.821 V16.1.0, “3rd Generation Partnership Project; Technical Specification Group Radio Access Network; Solutions for NR to support non-terrestrial networks (NTN) (Release 16),” 3GPP, techreport, May 2021.
- [2] X. Wang, W. Shen, C. Xing, J. An, and L. Hanzo, “Joint bayesian channel estimation and data detection for OTFS systems in LEO satellite communications,” *IEEE Transactions on Communications*, vol. 70, no. 7, pp. 4386–4399, 2022.
- [3] B. Shen, Y. Wu, J. An, C. Xing, L. Zhao, and W. Zhang, “Random access with massive MIMO-OTFS in LEO satellite communications,” *IEEE Journal on Selected Areas in Communications*, vol. 40, no. 10, pp. 2865–2881, 2022.
- [4] J. Guo, Y. Cui, C.-K. Wen, and S. Jin, “Prompt-enabled large AI models for CSI feedback,” *arXiv preprint arXiv:2501.10629*, 2025.
- [5] J. Feng, H. Q. Ngo, and M. Matthaiou, “Rectangular pulse-shaped OTFS with fractional delay and doppler shift for MU-MIMO systems,” in *2023 IEEE International Conference on Communications Workshops (ICC Workshops)*, May 2023, pp. 788–793.
- [6] R. Hadani, S. Rakib, M. Tsatsanis, A. Monk, A. J. Goldsmith, A. F. Molisch, and R. Calderbank, “Orthogonal time frequency space modulation,” in *2017 IEEE Wireless Communications and Networking Conference (WCNC)*, March 2017, pp. 1–6.

- [7] Y. Mao, O. Dizdar, B. Clerckx, R. Schober, P. Popovski, and H. V. Poor, "Rate-splitting multiple access: Fundamentals, survey, and future research trends," *IEEE Communications Surveys and Tutorials*, vol. 24, no. 4, pp. 2073–2126, Fourthquarter 2022.
- [8] P. Raviteja, K. T. Phan, Y. Hong, and E. Viterbo, "Interference cancellation and iterative detection for orthogonal time frequency space modulation," *IEEE Transactions on Wireless Communications*, vol. 17, no. 10, pp. 6501–6515, Oct 2018.
- [9] Z. Yuan, F. Liu, W. Yuan, Q. Guo, Z. Wang, and J. Yuan, "Iterative detection for orthogonal time frequency space modulation with unitary approximate message passing," *IEEE Transactions on Wireless Communications*, vol. 21, no. 2, pp. 714–725, 2022.
- [10] S. Li, W. Yuan, Z. Wei, and J. Yuan, "Cross domain iterative detection for orthogonal time frequency space modulation," *IEEE Transactions on Wireless Communications*, vol. 21, no. 4, pp. 2227–2242, 2022.
- [11] Z. Tie, J. Shi, S. Yan, K. Wu, and Z. Li, "Optimal power allocation for OTFS with frequency-domain linear equalizers," *IEEE Communications Letters*, vol. 26, no. 11, pp. 2715–2719, 2022.
- [12] S. Li, J. Yuan, P. Fitzpatrick, T. Sakurai, and G. Caire, "Delay-doppler domain tomlinson-harashima precoding for OTFS-Based Downlink MU-MIMO transmissions: Linear complexity implementation and scaling law analysis," *IEEE Transactions on Communications*, vol. 71, no. 4, pp. 2153–2169, April 2023.
- [13] B. C. Pandey, S. K. Mohammed, P. Raviteja, Y. Hong, and E. Viterbo, "Low complexity precoding and detection in multi-user massive MIMO OTFS downlink," *IEEE Transactions on Vehicular Technology*, vol. 70, no. 5, pp. 4389–4405, 2021.
- [14] B. Du, Y. Zhang, C. Masouros, and B. Clerckx, "Signal design for OTFS dual-functional radar and communications with imperfect CSI," *arXiv preprint arXiv:2510.20112*, 2025.
- [15] A. Sattarzadeh, O. Dizdar, V. Battula, and S. Wang, "Low-complexity precoder design for MU-MIMO OTFS networks," *IEEE Wireless Communications Letters*, vol. 14, no. 5, pp. 1301–1305, 2025.
- [16] B. Clerckx, Y. Mao, R. Schober, E. A. Jorswieck, D. J. Love, J. Yuan, L. Hanzo, G. Y. Li, E. G. Larsson, and G. Caire, "Is NOMA efficient in multi-antenna networks? A critical look at next generation multiple access techniques," *IEEE Open Journal of the Communications Society*, vol. 2, pp. 1310–1343, 2021.
- [17] B. Clerckx, Y. Mao, R. Schober, and H. V. Poor, "Rate-splitting unifying SDMA, OMA, NOMA, and multicasting in MISO broadcast channel: A simple two-user rate analysis," *IEEE Wireless Communications Letters*, vol. 9, no. 3, pp. 349–353, March 2020.
- [18] A. Mishra, Y. Mao, O. Dizdar, and B. Clerckx, "Rate-splitting multiple access for downlink multiuser MIMO: Precoder optimization and PHY-Layer design," *IEEE Transactions on Communications*, vol. 70, no. 2, pp. 874–890, 2022.
- [19] O. Dizdar, Y. Mao, and B. Clerckx, "Rate-splitting multiple access to mitigate the curse of mobility in (massive) MIMO networks," *IEEE Transactions on Communications*, vol. 69, no. 10, pp. 6765–6780, 2021.
- [20] J. Xu and B. Clerckx, "Max-min fairness and PHY-layer design of uplink mimo rate-splitting multiple access with finite blocklength," *IEEE Transactions on Communications*, vol. 73, no. 5, pp. 3671–3682, 2025.
- [21] Y. Xu, Y. Mao, O. Dizdar, and B. Clerckx, "Rate-splitting multiple access with finite blocklength for short-packet and low-latency downlink communications," *IEEE Transactions on Vehicular Technology*, vol. 71, no. 11, pp. 12 333–12 337, Nov. 2022.
- [22] J. Seong, J. Park, J. Lee, J. Lee, J.-B. Kim, W. Shin, and H. V. Poor, "Rate-matching framework for RSMA-enabled multibeam LEO satellite communications," *IEEE Transactions on Signal Processing*, vol. 73, pp. 1426–1443, 2025.
- [23] Y. Xu, L. Yin, Y. Mao, W. Shin, and B. Clerckx, "Distributed rate-splitting multiple access for multilayer satellite communications," *IEEE Transactions on Communications*, vol. 72, no. 10, pp. 6131–6144, 2024.
- [24] M. M. ahin, O. Dizdar, B. Clerckx, and H. Arslan, "Multicarrier rate-splitting multiple access: Superiority of OFDM-RSMA over OFDMA and OFDM-NOMA," *IEEE Communications Letters*, vol. 27, no. 11, pp. 3088–3092, Nov. 2023.
- [25] Q. Huai, W. Yuan, Y. Wu, and P. Fan, "Cross-domain transmission scheme for uplink OTFS-RSMA based on heterogeneous mobile user grouping," *IEEE Communications Letters*, pp. 1–1, 2024.
- [26] —, "Downlink OTFS-RSMA cross-domain transmission scheme and sum-rate maximization," *IEEE Communications Letters*, vol. 29, no. 3, pp. 600–604, 2025.
- [27] J. Liu, Y. Liang Guan, Y. Ge, and B. Clerckx, "Power allocation for high mobility OTFS-RSMA system with path-selective one-tap receiver," *IEEE Wireless Communications Letters*, vol. 14, no. 3, pp. 661–665, 2025.
- [28] H. Joudeh and B. Clerckx, "Sum-rate maximization for linearly precoded downlink multiuser MISO systems with partial CSIT: A rate-splitting approach," *IEEE Transactions on Communications*, vol. 64, no. 11, pp. 4847–4861, Nov. 2016.
- [29] Y. Mao, B. Clerckx, and V. O. Li, "Rate-splitting multiple access for downlink communication systems: Bridging, generalizing, and outperforming SDMA and NOMA," *Journal on Wireless Communications and Networking*, no. 133 (2018), 2018.
- [30] P. Raviteja, Y. Hong, E. Viterbo, and E. Biglieri, "Practical pulse-shaping waveforms for reduced-cyclic-prefix OTFS," *IEEE Transactions on Vehicular Technology*, vol. 68, no. 1, pp. 957–961, Jan 2019.
- [31] X. Zhou, K. Ying, Z. Gao, Y. Wu, Z. Xiao, S. Chatzinotas, J. Yuan, and B. Ottersten, "Active terminal identification, channel estimation, and signal detection for grant-free NOMA-OTFS in LEO satellite internet-of-things," *IEEE Transactions on Wireless Communications*, vol. 22, no. 4, pp. 2847–2866, 2023.
- [32] L. You, K.-X. Li, J. Wang, X. Gao, X.-G. Xia, and B. Ottersten, "Massive MIMO transmission for LEO satellite communications," *IEEE Journal on Selected Areas in Communications*, vol. 38, no. 8, pp. 1851–1865, Aug. 2020.
- [33] 3GPP TR 38.811 V15.4.0, "3rd Generation Partnership Project; Technical Specification Group Radio Access Network; Study on New Radio (NR) to support non-terrestrial networks (Release 15)," 3GPP, techreport, Sep. 2020.
- [34] Q. Ren, Y. Li, Z. Zhang, and S. Lu, "OTFS-SDMA for massive grant-free random access in leo satellite internet of things," *IEEE Transactions on Wireless Communications*, vol. 24, no. 8, pp. 6902–6916, 2025.
- [35] A. Papazafeiropoulos, B. Clerckx, and T. Ratnarajah, "Rate-splitting to mitigate residual transceiver hardware impairments in massive MIMO systems," *IEEE Transactions on Vehicular Technology*, vol. 66, no. 9, pp. 8196–8211, Sep. 2017.
- [36] P. Raviteja, K. T. Phan, and Y. Hong, "Embedded pilot-aided channel estimation for OTFS in delay-doppler channels," *IEEE Transactions on Vehicular Technology*, vol. 68, no. 5, pp. 4906–4917, 2019.
- [37] Y. Su, L. Jiang, and C. He, "Joint relay selection and power allocation for full-duplex df co-operative networks with outdated CSI," *IEEE Communications Letters*, vol. 20, no. 3, pp. 510–513, 2016.
- [38] D. Zhou, J. Guo, S. Wang, Z. Zheng, Z. Fei, W. Yuan, and X. Wang, "OTFS-based robust MMSE precoding design in over-the-air computation," *IEEE Transactions on Vehicular Technology*, vol. 73, no. 9, pp. 13 932–13 937, 2024.
- [39] A. Shapiro, D. Dentscheva, and A. Ruszczynski, *Lectures on Stochastic Programming: Modeling and Theory*. Philadelphia, PA: Society for Industrial and Applied Mathematics, 2021. [Online]. Available: <https://epubs.siam.org/doi/abs/10.1137/1.9781611976595>
- [40] S. S. Christensen, R. Agarwal, E. De Carvalho, and J. M. Cioffi, "Weighted sum-rate maximization using weighted MMSE for MIMO-BC beamforming design," *IEEE Transactions on Wireless Communications*, vol. 7, no. 12, pp. 4792–4799, 2008.
- [41] C. Shi, Y. Cui, Y. Chu, W. Yuan, and W. Guo, "Joint subcarrier and power allocation scheme for sum-rate maximization in OTFS-NOMA system," *IEEE Communications Letters*, vol. 28, no. 8, pp. 1889–1893, 2024.
- [42] S. Boyd and L. Vandenberghe, *Convex optimization*. Cambridge university press, 2004.
- [43] Y. Ye, *Interior point algorithms: theory and analysis*. John Wiley & Sons, 2011.
- [44] M. ApS, "Mosek optimization toolbox for matlab," *Users Guide and Reference Manual, Version*, vol. 4, no. 1, p. 116, 2019.
- [45] M. Grant, S. Boyd, and Y. Ye, "CVX: Matlab software for disciplined convex programming," 2008.